LA-UR- 97-2022

CONF-970276--8

Approved for public release; distribution is unlimited.

Title: CALIOPE AIRBORNE CO2 DIAL (CACDI) SYSTEM DESIGN

Author(s): Donald Mietz,NIS-4 David Thompson, CST-1
Bernie Archuleta,NIS-4 Joe Tiee, CST-6
Jake Archuleta,NIS-4 Mark Schmitt, XCM
Karla Atkins,NIS-3
Donald Bryd,NIS-4
Maureen Cafferty,NIS-4
Charles Fite,NIS-3
Paul Johnson,NIS-3
Bryan Laubscher,NIS-4
Nicholas Olivas, NIS-4

Submitted to: ITR, LAWRENCE LIVERMORE NATIONAL LAB
FEBRUARY 25-27, 1997

MASTER

DISCLAIMER

Los Alamos
NATIONAL LABORATORY

DISTRIBUTION OF THIS DOCUMENT IS UNLIMITED

CALIOPE Airborne CO_2 DIAL (CACDI) System Design

Don Mietz, Bernie Archuleta, Jake Archuleta, Karla Atkins, Don Byrd, Maureen Cafferty, Chuck Fite, Paul Johnson, Bryan Laubscher, Nick Olivas, Mark Schmitt, David Thompson, Joe Tiee

Los Alamos National Laboratory is currently developing an airborne CO_2 Differential Absorption Lidar (DIAL) system based on second generation technology demonstrated last summer at NTS. The CALIOPE Airborne CO_2 DIAL (CACDI) system requirements have been compiled based on the mission objectives and SONDIAL model trade studies. Subsystem designs have been developed based on flow down from these system requirements, as well as experience gained from second generation ground tests and N-ABLE (Non-proliferation AirBorne Lidar Experiments) airborne experiments. This paper presents the CACDI mission objectives, system requirements, the current subsystem design, and provides an overview of the airborne experimental plan.

I. Introduction

The CALIOPE Airborne CO_2 DIAL (CACDI) experiment is a continuation of the LANL investigation of performance characterization and validation of CO_2 DIAL systems in relation to the proliferation detection program. The CACDI mission will fly aboard the Argus aircraft which is managed by the Air Force, Phillips Laboratory LIMF, and operated by the Detachment 2, 452nd Flight Test Wing. The program is funded by the Department of Energy (DOE), Office of Nonproliferation and National Security. Initial flight testing of the CACDI system will begin in November 1997, and will conclude the summer of 1998.

This document describes the CACDI requirements needed to fulfill the experimental study of high repetition, low pulse energy transmitters, and high sensitivity receivers deemed necessary to realize future operational systems. The document opens by presenting the mission objectives and modeling optimization used to develop the CACDI system requirements. These requirements are summarized and then reduced to subsystem requirements presented within the descriptions of each major CACDI subsystem. Also presented is an overview of the CACDI experimental plans and the ground equipment required to support the CACDI airborne experiments.

II. Mission Objectives

A. Mission Goals

Execution of the CACDI test series is a crucial step in the fulfillment of CALIOPE's overall goal to advance the technology of CO_2 DIAL interrogation of effluent plumes for nuclear proliferation detection purposes. For the first time, the CACDI experiments will encompass all the relevant physics issues for

operational, nonproliferation detection missions. The lidar subsystems being developed for these experiments continue the evolution of technologies that will allow future deployment of autonomous systems with higher detection sensitivity and greater standoff range.

B. Operational Issues

Performing proliferation detection from a remote airborne platform dictates that the lidar system be configured to deal with several unavoidable operational issues. First, the lidar must view the target from a moving platform through many kilometers of ambient atmosphere. Thus, variations in the characteristics of the atmosphere occurring during the observation time will produce variations in the collected data. To minimize the effects of these variations on the lidar detection sensitivity requires that the variations be sampled equally by all wavelengths. This is being accomplished by using acousto-optic deflectors that can tune the laser frequency at rates equal to the fastest pulse rate of the laser.

Secondly, the plumes from proliferation facilities will have their highest concentration at their source, where the plume's cross-section is small. In order to achieve maximum absorption of the lidar beam by the plume, the beam diameter at the target must also be small (typically 10 meters or less). Consequently, the speckle noise on the return signal will be high, necessitating multiple-pulse averaging to achieve high detection sensitivity. This drives the design of the lidar system to a high repetition rate configuration where the pulse frequency at any single wavelength is determined by the speed of the platform and the size of the receiving aperture. The design of the CACDI lasers will allow the collection of data at the maximum allowed pulse rate over a wide spectrum of laser lines.

As the pulse rate of the laser rises in order to achieve maximum shot averaging over as many laser lines as possible, the average power requirements of the laser also rise. The prime power requirement of the laser is dictated by the laser efficiency, the laser repetition rate and the output pulse energy. The maximum available power to run the laser is set by the power generation limitation of the platform. In order to remain within this power constraint envelope, the minimum pulse energy required to achieve the speckle-limited SNR should be used. This minimum energy scales with the detection sensitivity of the receive. Through proper receiver design and the use of fast filtering technology, the required pulse energy of the laser can potentially be reduced by several orders-of-magnitude. The CACDI receiver is an initial step in this direction.

Finally, one must insure that the lidar system is able to evaluate regions of interest for their proliferation potential. This type of analysis includes detection of regions of interest, evaluation of a specific location with respect to neighboring regions, and the proper chemometric analysis of the collected data to determine which chemicals are present. Such analyses require a synthesis between data collection and data analysis. During the CACDI test series, data will be collected to perform differential spatial analysis

of plume data and focal plane array data (from a ground based imager). Analysis techniques will be analyzed for their effectiveness in locating plumes and in determining their concentration.

III. System Requirements

A. Summary

Simulations were run (SONDIAL input file CACDI001-006) for the CACDI system. Parameters used in the calculations are given in Table 1. The predicted signal-to-noise (SNR) is given in Figure 1 versus range and in Figure 2 versus divergence for operation at 20 km on the $^{13}C^{18}O_2$ 10P20 line. A single-pulse SNR of 4.2 is achieved for this line at 20 km. Performance using the $^{12}C^{16}O_2$ laser is degraded owing to increased atmospheric CO_2 absorption. The predicted SNR for the 10P20 line of the $^{12}C^{16}O_2$ laser as a function of range is given in Figure 3 and has a value of 2.1 at 15km range. Optimum performance of the system depends heavily on the ability of the transmitter to provide the assumed pulse energy, the receiver to operate at the stated noise level, and the ability to achieve the timing stability commensurate with operation of the pulse integration electronics at an effective gate width of 500 ns or less. Since some of the CO_2 laser wavelengths with low gain will have pulse widths in excess of 500ns, it has been assumed that operation at 20km will use only lines with high gain.

B. Transmitter Model

The lasers are assumed to generate 2 mJ of output energy in the TEM_{00} mode. Vignetting losses in the transmitter optics are calculated using the mirror to spot size ratio, α. The fractional transmission, F_{out} is given by

$$F_{out} = 1 - e^{-\alpha^2}$$

which gives a transmission of 99% for α=3. To account for additional losses caused by optical elements in the transmitter and receiver beam lines, a transmission efficiency of 40% was assumed. This number is identical to that calculated for the N-ABLE experiment. These losses reduce the effective laser energy for a loss-less lidar system to 790 μJ. The laser was assumed to be running on the $^{13}C^{18}O_2$ 10P20 line where the round trip atmospheric transmission is about 50 %. Operation at many of the 9P and 9R lines will be degraded owing to additional losses from ozone absorption. A single line repetition rate of 1000 Hz and a system jitter of 50 μrad were assumed for the system calculation.

Table 1. List of parameters for the CACDI experiment.

Parameter	CACDI Value and Units
Pulse energy	2 mJ
Pulse length	200-400 ns
Wavelength (nominal)	10 μm ($^{12}C^{16}O_2$ and $^{13}C^{18}O_2$ lines)
Repetition rate (each laser)	5000 Hz
Pointing Jitter	50 μrad
Transmitter mirror diameter	10.16 cm
Transmitter divergence	0.5 mrad (maximum)
Xmitter vignetting loss	0.01
Mirror to spot size ratio	3
Receiver fractional obscuration	.333
Receiver mirror size	30.5 cm
Receiver effective f number	0.9
Optical efficiency	0.4
Optical bandwidth	2.0 μm
Preamplifier bandwidth	1.0 MHz
Amplifier NEP	50 pW
Detector efficiency	0.8
Detector temperature	51 °K
Detector size	200 μm by 200 μm
Target reflectivity (surf. norm.)	3 %
Line of sight from horizontal	-20°
Range to target	20 km
Atmospheric Model	Standard 76, 23 km Visibility
Optical spot size at target	10 m
SNR (single-shot)	4.2 (at most Isotopic10P lines)

C. Receiver Model

The Generation II detector/amplifier has a measured noise equivalent power (NEP) of 39 pW when viewing a cold (77° K) plate. This value was rounded to 50 pW for the CACDI simulations. SONDIAL calculates the photon flux noise from the 300° K background scene separately. An effective integration time of 500ns (for a Nyquist bandwidth of 1.0 MHz) was assumed. Using an NEP of 50 pW, the NEI of the detector/amplifier pair is

$$NEI = \frac{\lambda}{hcA_d} NEP = \frac{5\text{x}10^{19}}{A_d} NEP = 1.25\text{x}10^{27}\, NEP = 6\text{x}10^{16} \text{ photons/m}^2\text{sec.}$$

The detector was assumed to be 200 mm × 200 mm square. A temperature of 51°K was used to calculate the detector thermal noise and 1/f noise (whose affects are negligible). The dominant noise sources are shot noise (100 pW at 20km) and amplifier noise (50pW).

D. Simulation results

The predicted SNR performance of the CACDI system versus range is shown in Figure 1. The results show that a system SNR of 4.2 is achieved with 2 mJ of $^{13}C^{18}O_2$ laser power at 20 km range with a beam divergence of 0.5mrad. This corresponds to filling about 75% of the detector field of view with the laser spot. Many of the isotopic lines have SNRs exceeding 4, while the conventional CO_2 lines never exceed an SNR of 2, owing to the increased absorption by atmospheric CO_2 (by a factor of about 3-4). The performance of the system versus range using the 10P20 line of the $^{12}C^{16}O_2$ laser is shown in Figure 3. Plots of the SNR at each laser line are given in Figures 4-11 for the $^{13}C^{18}O_2$ laser at 20 km and the $^{12}C^{16}O_2$ laser at 15 km.

Optimum performance of the system with the $^{12}C^{16}O_2$ laser would be achieved using a smaller detector, at the expense of degraded performance of the $^{13}C^{18}O_2$ SNR (and assuming the smaller detector could be aligned properly).

Based on these simulation results the requirements presented in Table 2 have been levied on the CACDI system.

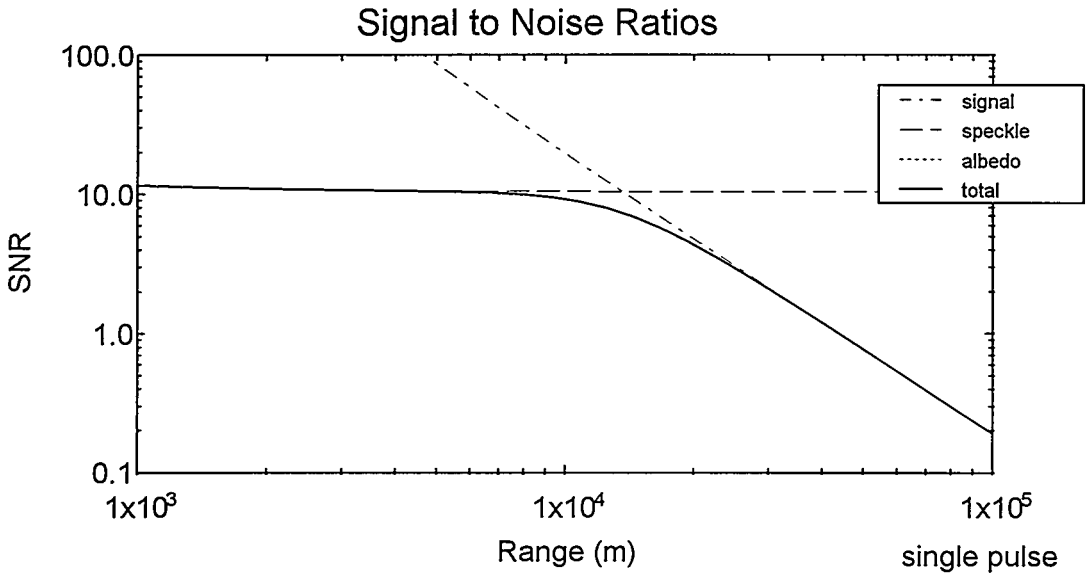

Figure 1. Plot of the CACDI SNR as a function of range to the target for the 10P20 line of the $^{13}C^{18}O_2$ laser.

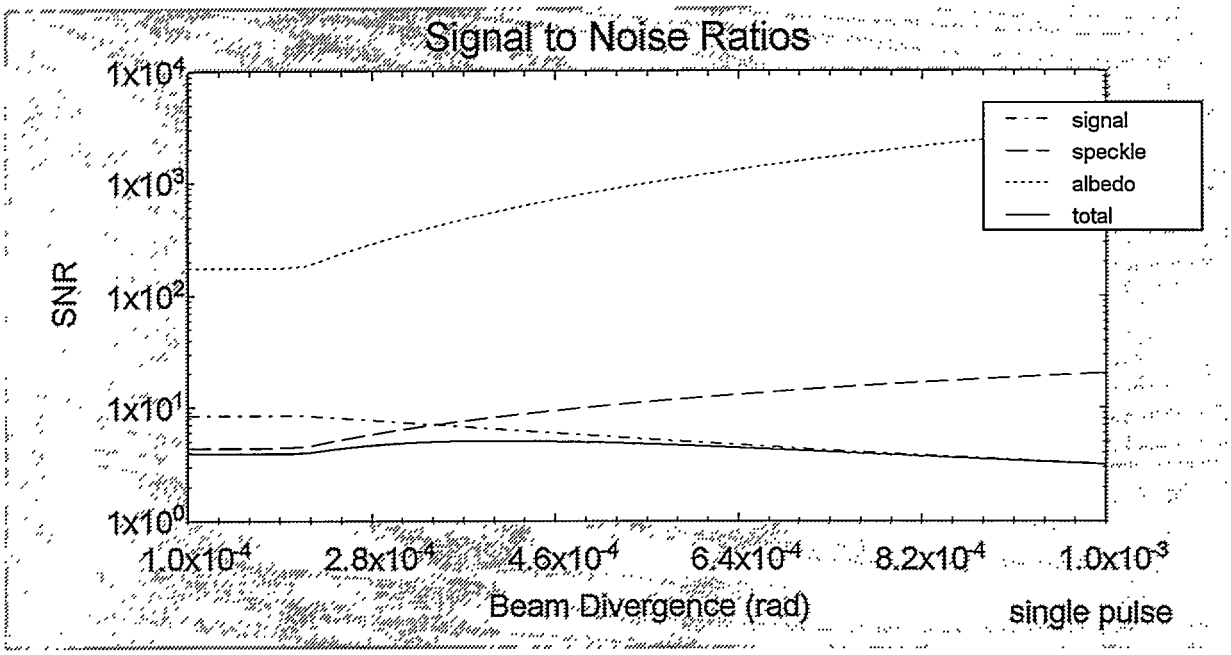

Figure 2. CACDI system SNR as a function of beam divergence (with optimum detector size for each possible divergence) for operation at 20 km. Note that optimum performance is achieved at 0.43 mrad.

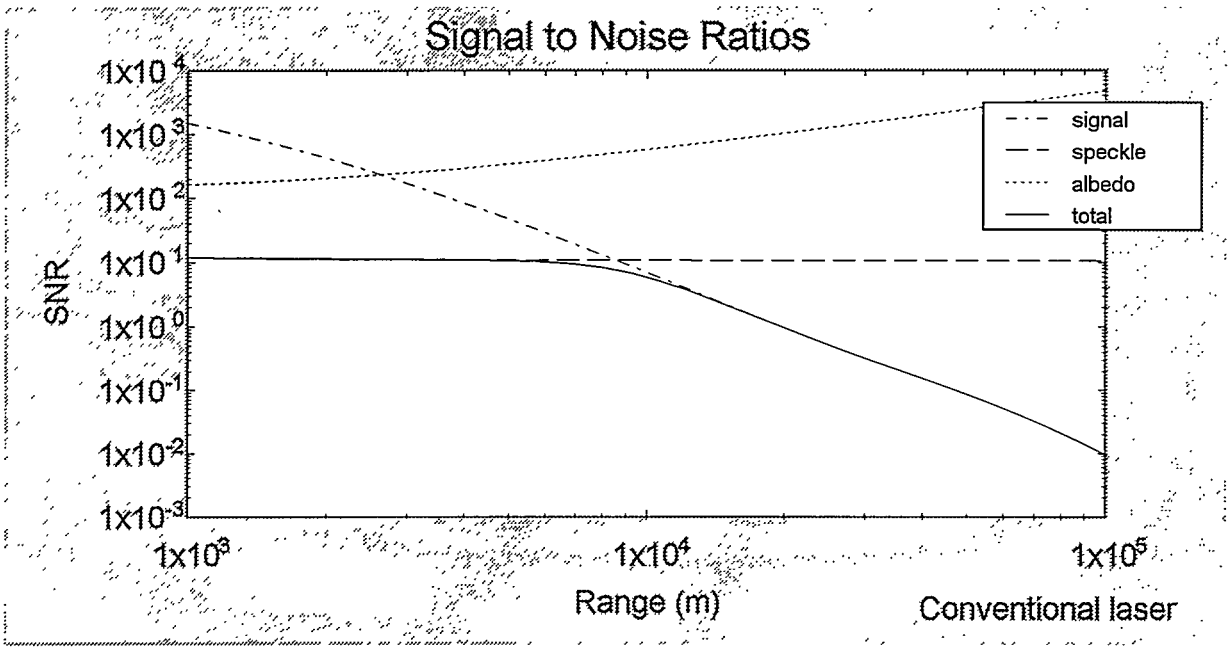

Figure 3. Signal to noise ratio for the 10P20 line of the $^{12}C^{16}O_2$ laser. Performance is degraded with respect to the $^{13}C^{18}O_2$ laser owing to increased atmospheric CO_2 absorption.

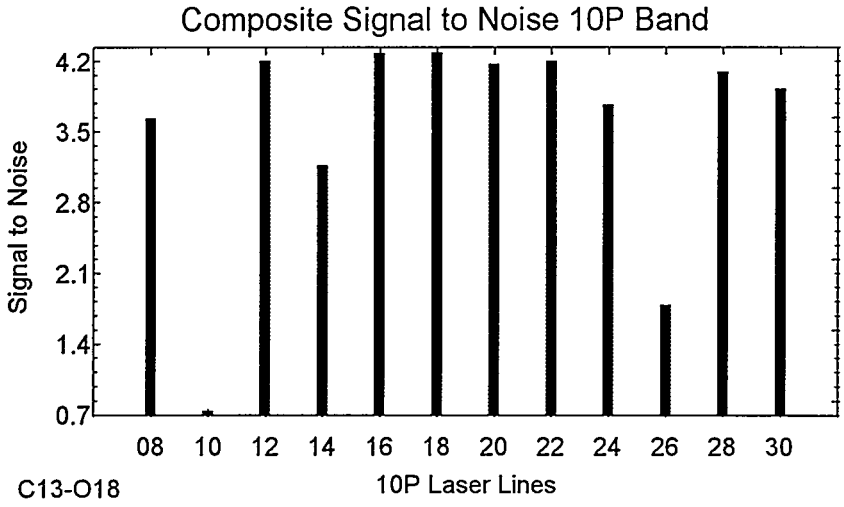

Figure 4. SNR for the 10P branch wavelengths of the $^{13}C^{18}O_2$ laser at a range of 20 km.

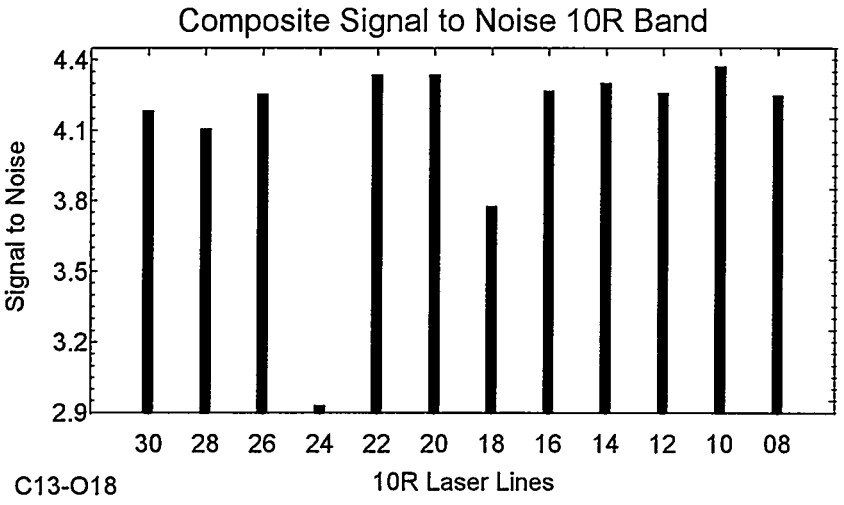

Figure 5. SNR for the 10R branch wavelengths of the $^{13}C^{18}O_2$ laser at a range of 20 km.

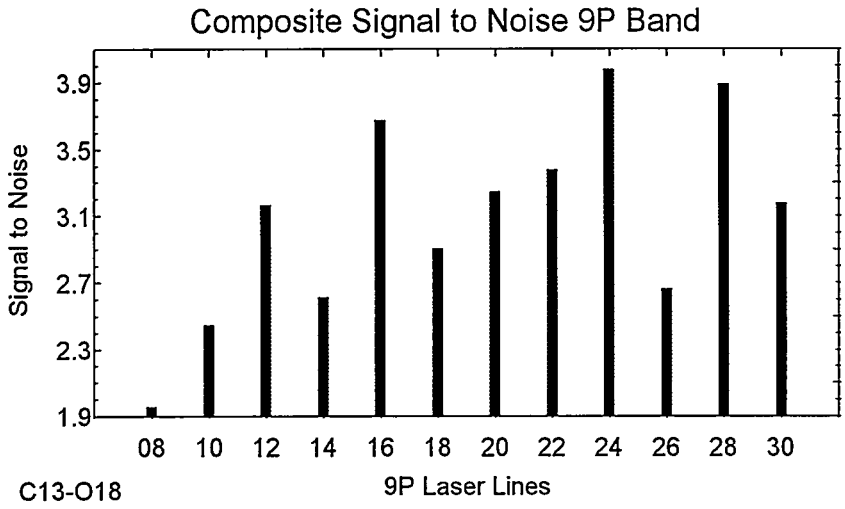

Figure 6. SNR for the 9P branch wavelengths of the $^{13}C^{18}O_2$ laser at a range of 20 km.

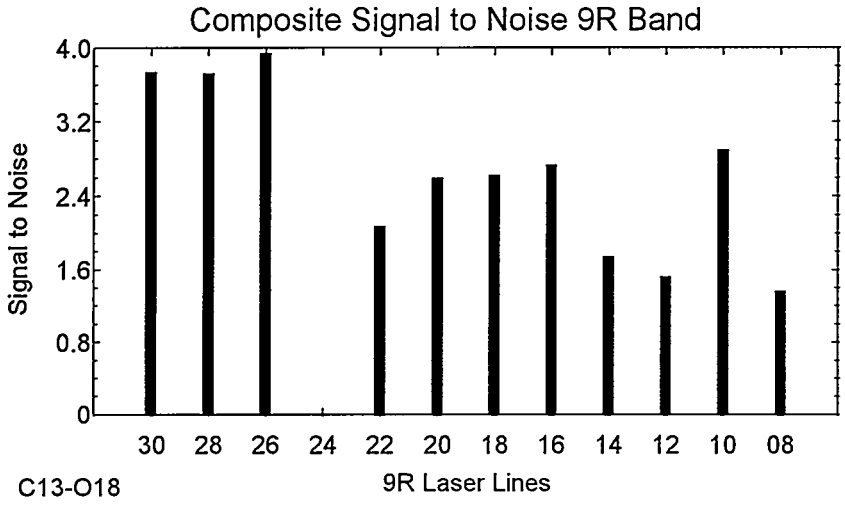

Figure 7. SNR for the 9R branch wavelengths of the $^{13}C^{18}O_2$ laser at a range of 20 km.

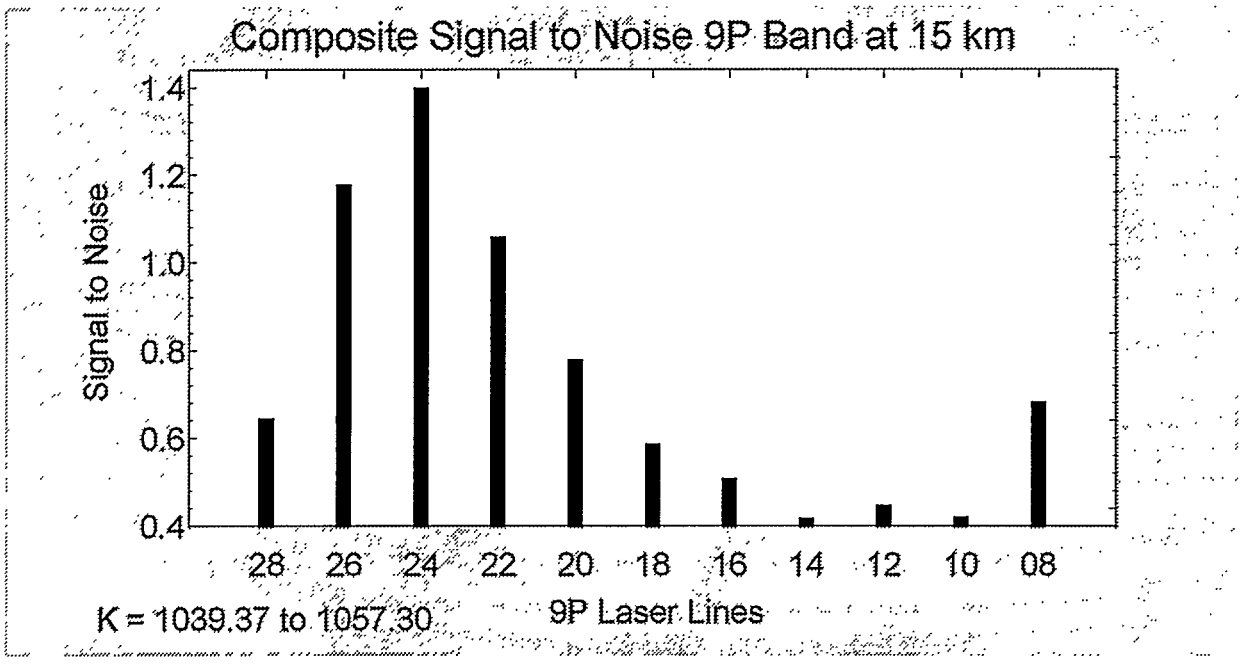

Figure 8. SNR for the 9P branch wavelengths of the $^{13}C^{16}O_2$ laser at a range of 20 km.

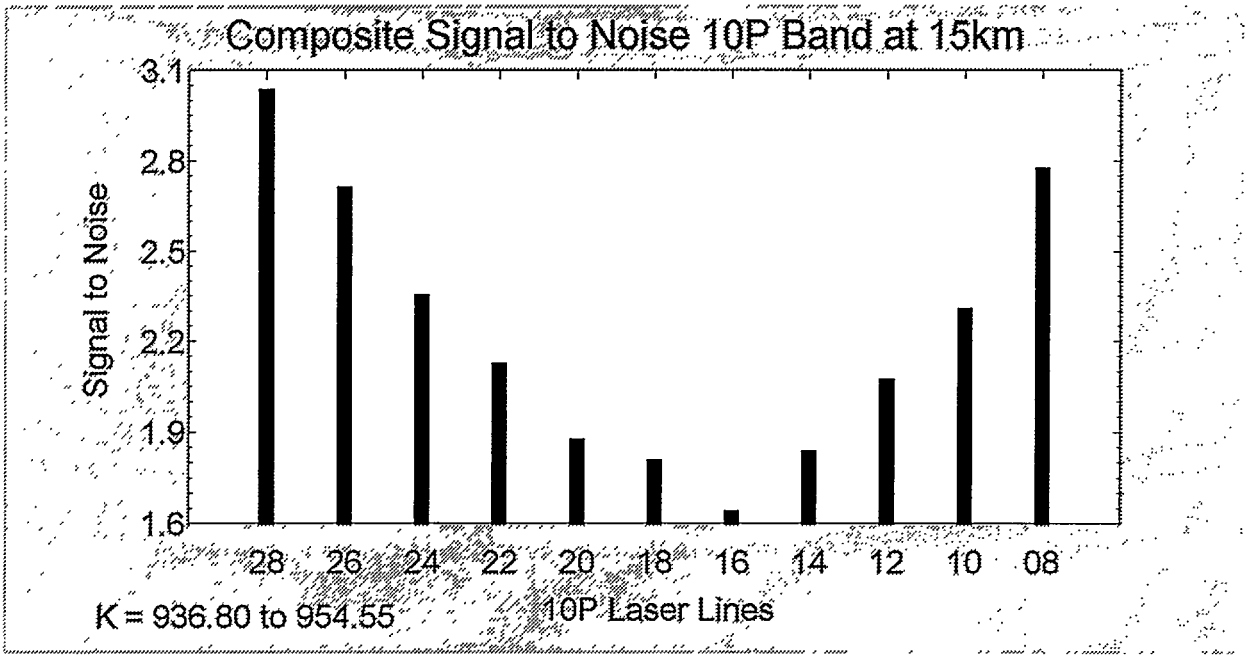

Figure 9. SNR for the 10P branch wavelengths of the $^{12}C^{16}O_2$ laser at a range of 15 km

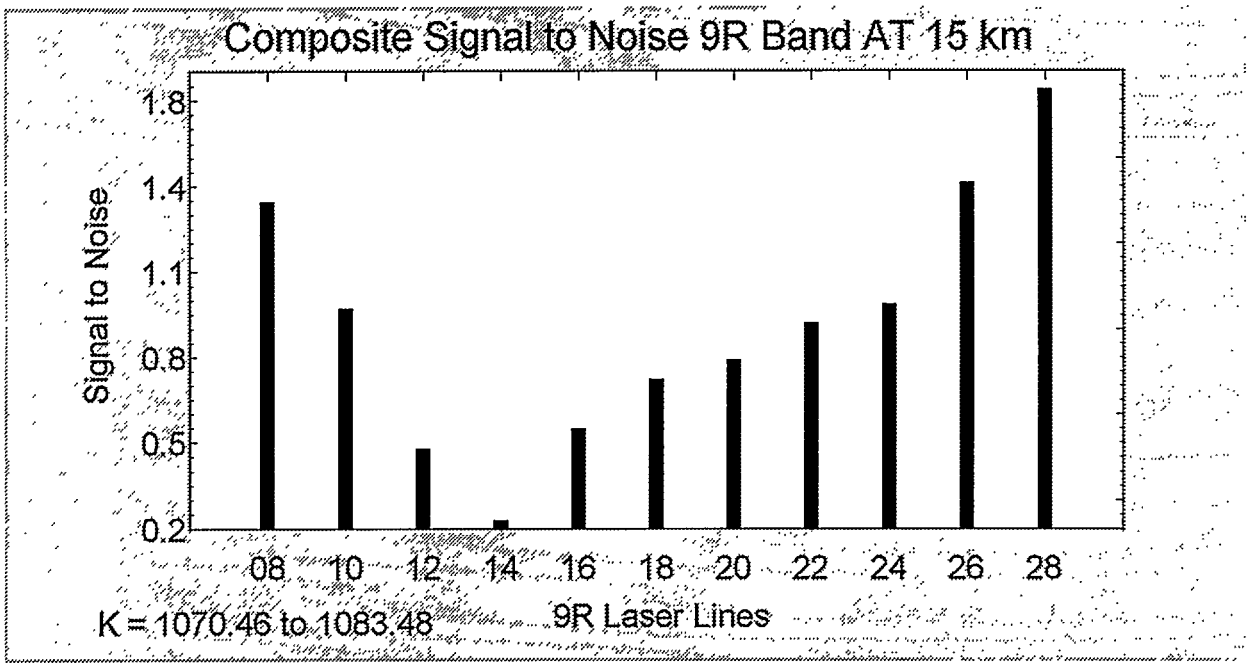

Figure 10. SNR for the 9R branch wavelengths of the $^{12}C^{16}O_2$ laser at a range of 15 km.

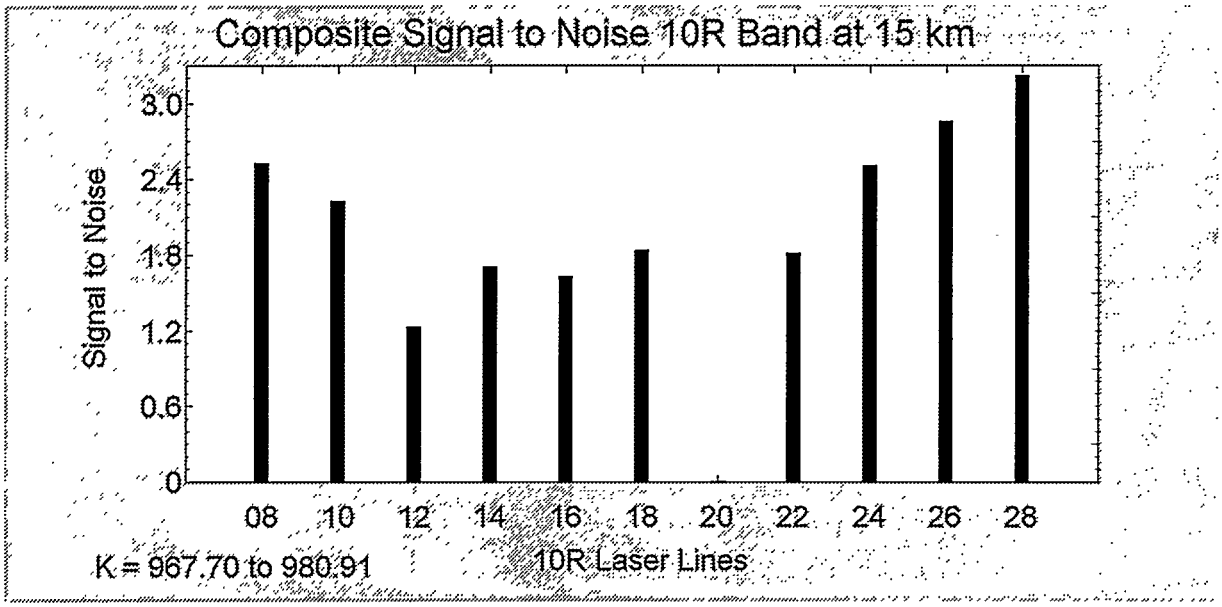

Figure 11. SNR for the 10R branch wavelengths of the $^{12}C^{16}O_2$ laser at a range of 15 km.

Table 2. List Of CACDI System Requirements

Requirement Description	Quantitative Value/Units
Line of Sight (LOS) Slant Range	7.5 to 20 km
Number of Lasers/CO_2 Isotope	2 lasers, $^{12}C^{16}O_2$ & $^{13}C^{18}O_2$
Pulse Energy	2 mJ Nominal
Pulse Width	200 to 400 ns
Repetition Rate	Two Pulse Burst, with a Burst Rate of 5 kHz
Wavelength Tuning Rate	Each Laser is AC tuned at 5 kHz
Divergence	200 to 500 μrad
Receiver Aperture	30.5 cm
Receiver Effective *f*#	*f*1
Receiver Field-of-View (FOV)	665 μrad
Common & Differential Mode Jitter	+ 50μrad
Detector Element Size	200 μm
Stirling-Cycle Cryostat Operating Temperature	35° K
Maximum System Optical Bandwidth	9.0 to 11.5 μm
Receiver Noise	50 pW or less
Integration Temporal Gate Width	500 ns
Slant Range Knowledge	50 ns

IV. System Configuration and Overall Project Schedule

A. General Information

Figure 12 illustrates the three major elements of the CACDI system; the DAC (data acquisition and control) Pallet, the Optics Assembly Bench (main optics bench), and the Laser Support Pallet. An isometric view of the CACDI system aboard the Argus aircraft is shown in Figure 13.

The Optics Assembly Bench provides a stable, flexible substrate to mount the receiver, transmitter, gimbaled mirror, alignment optics, and required support equipment. The optical bench is supported by four air isolators; one at each corner. The isolators are attached on the bottom side to a pallet which in turn is attached to the Argus floor rails.

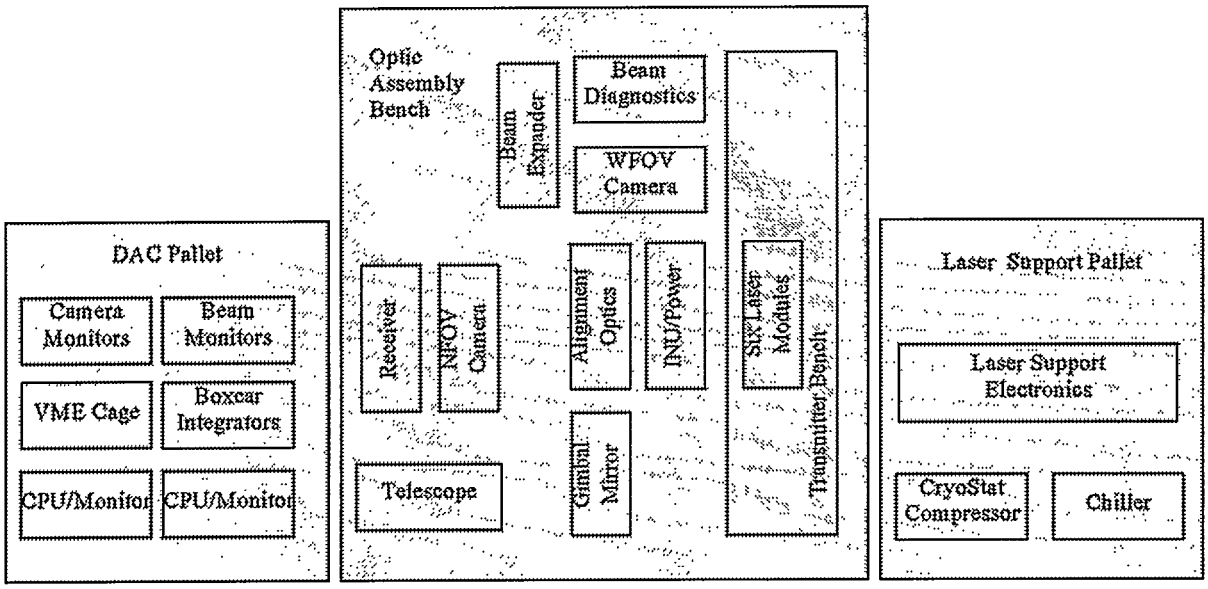

Figure 12. Block Diagram of the CACDI Components

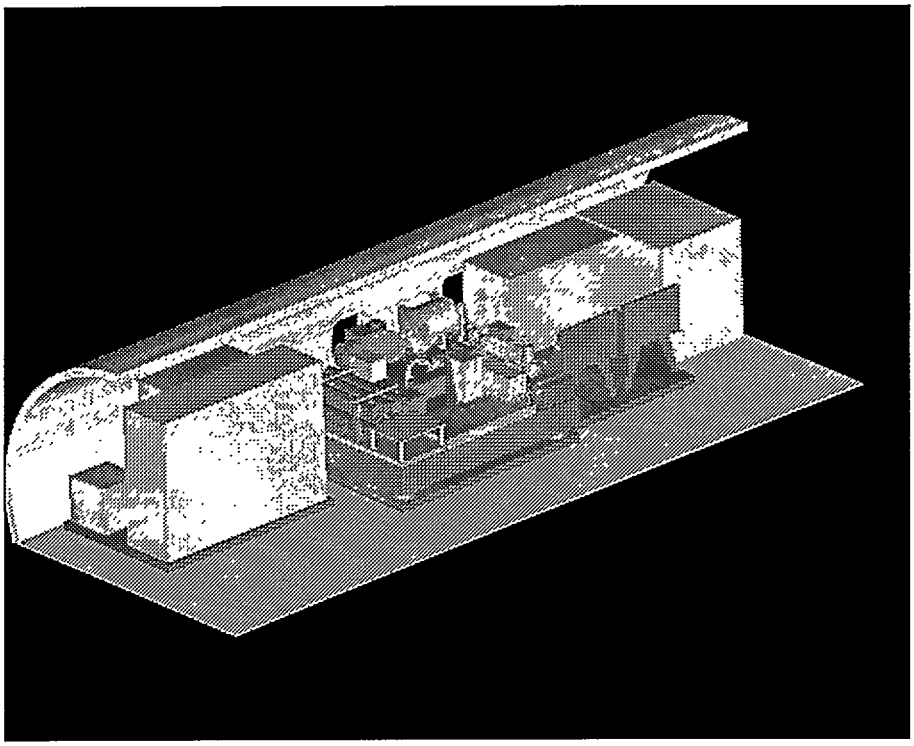

Figure 13. Isometric View of the Optic Assembly Bench Within the Argus Aircraft

The DAC Pallet, located forward of the optical bench, is a plate that supports the equipment rack for the DAC, as well as the two chairs for the CACDI system operator and on-board data analyst. The DAC rack holds the Sun Computer CPU units, display monitors, data storage unit, VME cage for the real-time processing and I/O modules, a NIM Bin for the boxcar integrators, and several monitors for viewing beam diagnostics and the acquisition camera images.

The Laser Support Pallet is located aft of the optical bench. This pallet contains a chiller for cooling the laser modules and RF drives, a compressor for driving the receiver mechanical cooler, and a 3 bay equipment rack for laser power and control electronics.

The location of the Argus optical windows can be varied within the aircraft main cargo door. CACDI will use the aft window location, centered at Station 518. Use of the aft window allows placement of the DAC forward of the assembly bench, separating the high voltage laser RF signals from the sensitive analog data signals.

B. Optics Tables

The CACDI system uses an assembly bench which is 96 inches long (oriented fwd-aft on the aircraft), 87 inches wide (oriented inbd-outbd), and 12.12 inches thick. The top, bottom and side surfaces are 0.19 inch thick 400SS plate. The top surface is tapped with 0.25-28UNF thread on a one inch spacing with a 1 ½" boundary along the outside edge.

Three small breadboards are used; one mounts the transmitter laser modules and supporting optical components (Breadboard 'B'), the second mounts the beam conditioning, diagnostics and expander (Breadboard 'C'), and the third mounts the receiver relay tube, beam splitter and narrow field of view (NFOV) acquisition camera and its optics (Breadboard 'D').

C. Transmitter

Six laser modules are mounted in an aluminum cradle designed to allow module thermal growth in the axial direction. The cradle is attached to breadboard 'B' by 4 mounts which provide stability in the inboard-outboard aircraft axis.

Two manifolds distribute the cooling fluid from the chiller to the laser modules. Flexible hydraulic hoses, routed near the aircraft floor, complete the hydraulic circuit from the Optic Assembly Bench to the chiller.

D. Receiver

The receiver and the relay tube are mounted on translation stages that allow axial and transverse horizontal adjustments. Limited rotations about the transverse axes as well as small vertical adjustments are provided by a kinematic mounting plate.

Compressed Helium is delivered to the cryostat through 2 wire braided hoses that are routed upward from the receiver to a disconnect junction in the aircraft cable tray, then routed aft to the Laser Support Pallet and down to the compressor.

E. Optic Assembly Bench miscellaneous

Two alignment systems are mounted onto the table. The alignment fixture used for the receiver is mounted on breadboard 'D". The laser/receiver alignment fixture is located in the center of the main table. The gimbaled mirror has been modified to allow rotation of the optic past normal to the aircraft body, (i.e., facing inboard). The gimbaled mirror thus becomes part of the laser/receiver alignment subsystem.

A wide field of view (WFOV) camera, mounted to the assembly table "A", is located near the laser transmitter, and a narrow field of view (NFOV) camera is located within the receiver optical train, on breadboard 'D".

F. Laser Support Pallet

Dimensions of the Laser Support Pallet are 76 inches, fore-aft, by 60 inches, inboard-outboard, by 3.625 height. The pallet is located between Station 588 and Station 665 on the Argus aircraft. The pallet is located such that it permits access to the cargo door and the CACDI laser modules, located on the Optic Assembly Bench. Mounted on the pallet are:

- CTI-CRYOGENICS compressor,
- POLARPURE chiller,
- Three bay equipment rack for laser support electronics.

Manifolds mounted on the pallet direct waste chill water from the laser modules to the rack mounted power supply units.

G. Overall CACDI Schedule

Figure 14 presents the overall CACDI schedule. The highlights of the schedule include the following:

- System design development occurs from the present through the end of May 1997
- Integration and test of the of the CACDI system in Building 34 at TA-35 will occur during the three month period of April through June 1997
- Integration into a 10 foot wide semi-trailer, transport to TA-33, and performing ground field testing of the CACDI system occurs during the three month period of July through September 1997.
- Transport to Kirtland AFB, integration and check of the CACDI system aboard the Argus aircraft will occur during the month of October 1997
- First block of flight experiments performed locally in NM will occur during the month of November 1997.
- Second block of flight experiments at NTS occurring during the month of May 1998.

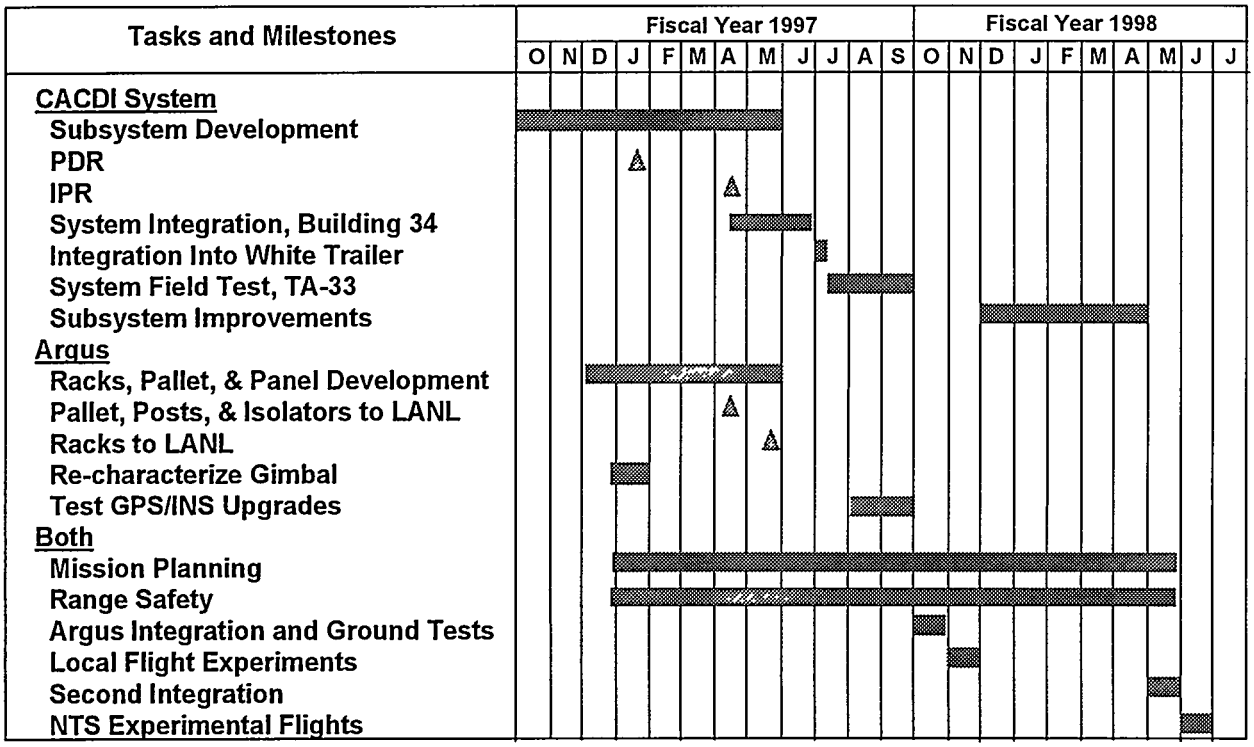

Figure 14. CACDI Top Level Schedule

V. Transmitter

A. General Description

The CACDI transmitter consists of two CO_2 laser systems, each in a master oscillator/amplifier (MOPA) configuration. One of these (Laser 0) uses normal CO_2 ($^{12}C^{16}O_2$) while the other (Laser 1) uses isotopic CO_2 ($^{13}C^{18}O_2$). The beams of these two lasers are combined and spatially filtered. A small portion of each beam is split off to diagnostics which include the DIAL reference detector. The beam is expanded in size with a 10X magnification beam expander. The beam then passes through a dichroic beam splitter after which it is directed to the gimbaled mirror by the telescope pick-off mirror and becomes co-axial with the receiver. Figure 15 is a block diagram of the transmitter, while Figure 16 shows an isometric view of the laser module cradle and adjacent optical bread boards.

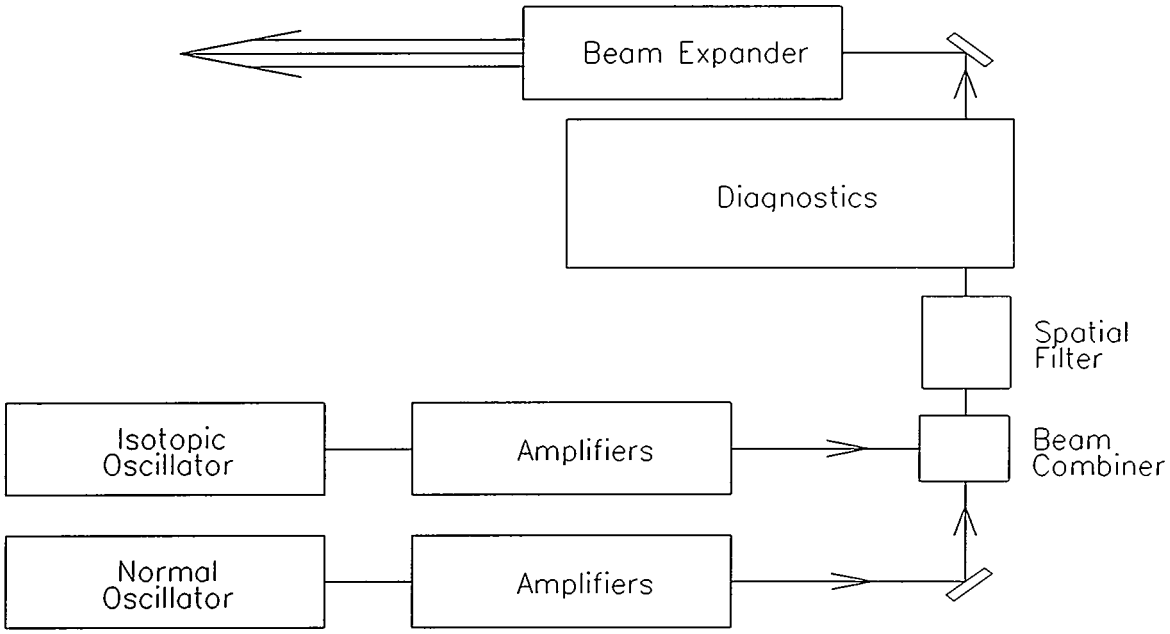

Figure 15. Transmitter Block Diagram

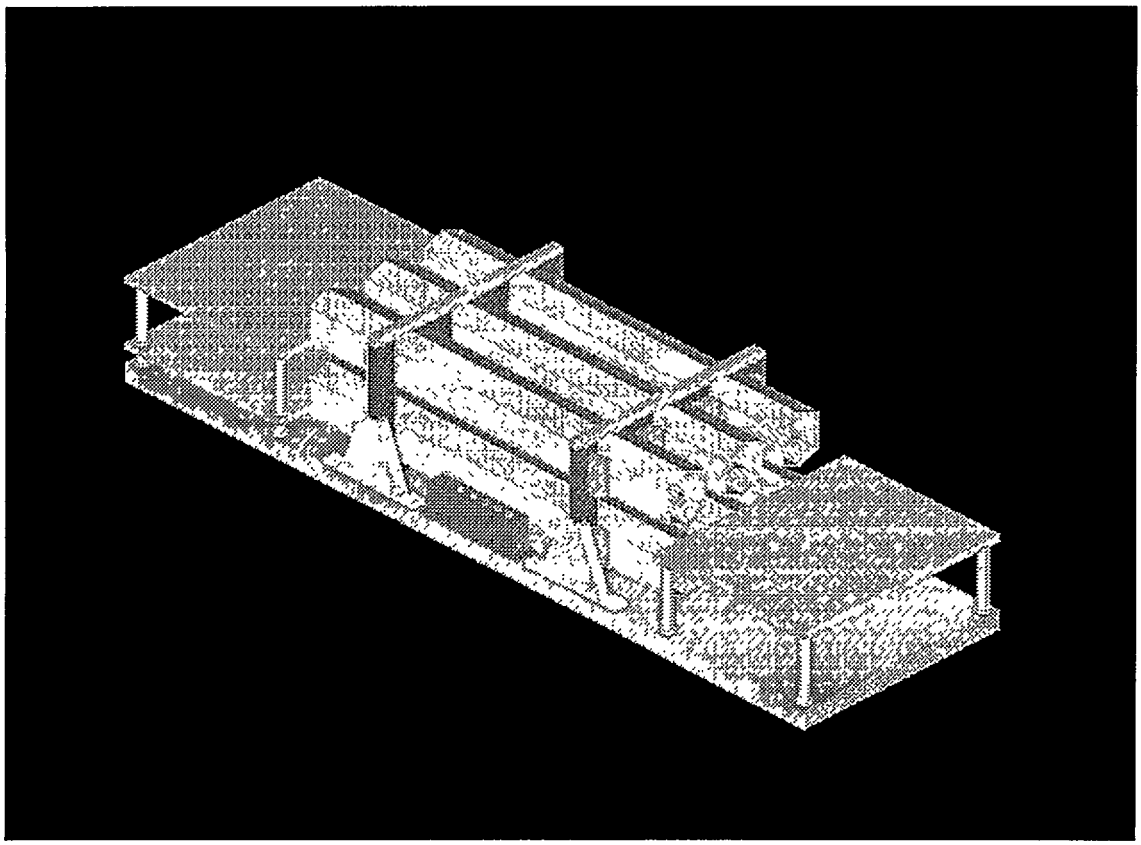

Figure 16. Isometric View of the Transmitter on the CACDI Optic Assembly Bench

The 6 Synrad laser gain modules which are used for the laser oscillators and amplifiers are held in a 2-high, 3-wide "laser cradle" on the 24" X 84" laser breadboard (Table "B"), with associated components for tuning, beam transport, and beam combining mounted on smaller 24" × 19" breadboards at each end of the cradle. The lower three modules form Laser 0 (the $^{12}C^{16}O_2$ or normal laser), while the upper three modules form Laser 1 (the $^{13}C^{18}O_2$ or isotopic laser). Components comprising the spatial filter, beam diagnostics and beam expander are mounted on the 24" X 48" diagnostics breadboard (Table "C").

B. Requirements

Table 4 below presents the transmitter subsystem requirements and the corresponding performance as measured in the laboratory.

Table 4, Transmitter Subsystem Requirements

	CACDI Requirement	CACDI Performance	
Number of lasers:	2	2	
Isotopes:		$^{12}C^{16}O_2$	$^{13}C^{18}O_2$
Repetition rate each laser [kHz]:	5	5	5
Tuning rate each laser [kHz]:	5	5	5
Pulse energy [mJ]:	2	2.5	2
Energy stability [%]:		2-5	2-5
Pulse width [ns]:	200-500	150-300 FWHM	200-400 FWHM
Pulse width stability [ns]:	±20	±20	±20
Pulse timing stability [ns]:	±20	±20	±20
Gaussian beam diameter [mm]:	67-100	67-100	67-100
Output beam divergence [μrad]:	150-300	150-300	150-300
Pointing stability [μrad]:	±20	±20	±20
Mode size stability [%]:	±10	±10	±10
M_2 parameter:	1.2	1.2	1.2

C. Description of Acousto-Optic Tuning

Acousto-optic tuning, as implemented in the CACDI transmitter, is performed by a pair of acousto-optic modulators, as shown conceptually in Figure 17

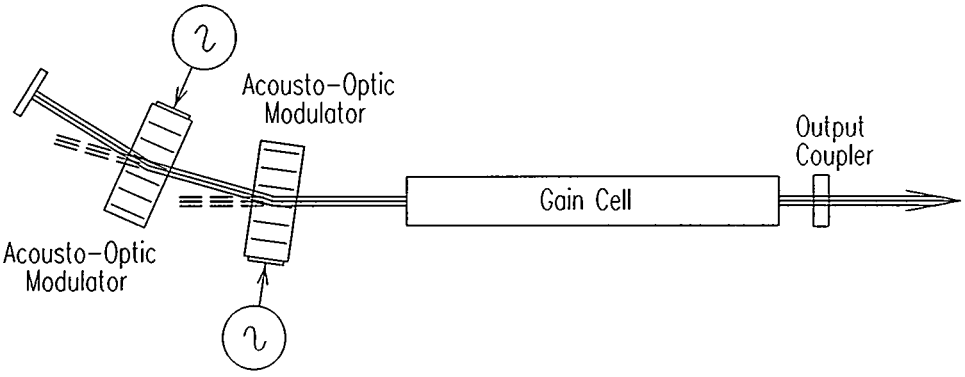

Figure 17. Acousto-Optic Tuning Concept

A radio-frequency acoustic wave is launched by a piezo-electric transducer into an optically transparent medium, in this case Germanium. The acoustic wave, at a frequency of about 80MHz, forms a traveling index grating in the modulator. Light waves incident on this grating can be efficiently scattered, with a deflection angle θ given by

$$\sin(\theta/2) = \lambda/2\Lambda$$

where λ and Λ are the optical and acoustic wavelengths, respectively. With the correct amplitude acoustic wave, over 97% deflection efficiency has been demonstrated. The deflected wave is either up-shifted or down-shifted in frequency, depending on direction relative to the acoustic wave. By using a pair of AO devices, the net frequency shift can be eliminated; otherwise light in the laser resonator would rapidly shift off the CO_2 resonance and no lasing could occur. Since the resonator fixes the direction of the optical beams and thus the deflection angle, it can be seen that as the acoustic frequency, and thus the acoustic wavelength, changes so must the optical wavelength. Thus the laser wavelength can be electronically tuned, with the response time limited only by the finite propagation time of the acoustic wave across the optical beam. This transit time is 5.5μs/mm, the acoustic velocity in Ge. As with a grating, the spectral resolution is determined by the number of grating lines illuminated - where each wave of the sound field can be thought of as a grating line. With two devices, each doubled-pass, the number of grating lines, and the spectral resolution, is multiplied by four. The overall resolution is determined by the ratio of the size of the beam parallel to the acoustic (horizontal) direction to the acoustic wavelength. Since the acousto-optic interaction in Ge is highest between a longitudinal acoustic wave and an optical wave polarized parallel to the acoustic propagation direction, the modulators and the oscillator gain cells are oriented so that the acoustic propagation and the light polarization are parallel.

D. General Descriptions of Laser Oscillator/Amplifiers

Figure 18 shows the layout of the two lasers, together with the small breadboards at each end of the laser cradle. Due to the "Z-folded" gain medium in the Synrad gain modules, the inputs and outputs are at different heights, separated by 2". The arrangement of the small breadboards permits optical components to be mounted within 3-3.5" of the breadboard surface.

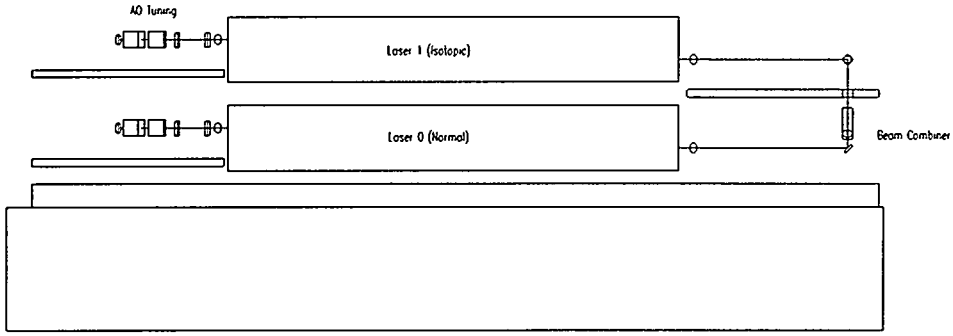

Figure 18. Layout of the Two Laser Transmitters

E. Description of Normal Isotope Oscillator

Figure 19 shows a schematic of the oscillator. The resonator is formed by a 65% reflectivity output coupler mounted to the gain module and a high reflector. The gain module is a Synrad model 60, which consists of a "Z-fold" of 3 channels each 1.0m long with a 6mm square cross section, for a total gain length of 3.0m. The module is filled with approximately 50 Torr of gas mix (2 Torr Xe / 6.6 Torr CO_2 / 6.6 Torr N_2 / balance He) and pumped with 3 kW (peak) of 40.68 MHz RF at a duty cycle of up to 50%. Tuning is accomplished by a pair of Isomet Model 1208-6 acousto-optic modulators. In order to improve the spectral resolution of the tuning, an afocal cylindrical telescope formed by ZnSe cylindrical lenses of -2" and +5" focal lengths expands the beam by a factor of 2.5 in the horizontal direction between the gain module and the first AO modulator. The AO modulators also operate as the Q-switch: by modulating the RF input to the modulators, the cavity loss can be rapidly switched from very high to very low, forming a Q-switched pulse. The tail of the pulse can be "clipped" by turning the loss back on.

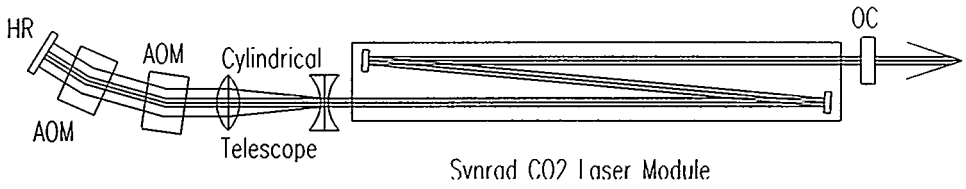

Figure 19. Schematic of an AO-Tuned Oscillator

F. Description of Normal Isotope Amplifiers

The oscillator output is amplified by a pair of single-pass amplifiers, each consisting of a single Synrad model 60 module. The light passes from the output of the oscillator to the input of the first amplifier, and from the output of the first amplifier to the input of the second amplifier, using a pair of mirrors located as close to the laser modules as possible, in order to minimize diffraction losses between modules.

G. Description of Isotopic Oscillator

The isotopic oscillator is identical to the normal isotope oscillator, except for the use of $^{13}C^{18}O_2$ in the gas fill. This isotope was chosen for its balanced gain characteristics. Tests indicate that gain reduction caused by oxygen exchange with the laser structure is not a problem.

H. Description of Isotopic Amplifiers

The isotopic amplifiers and associated optics are identical to those for the normal isotope amplifiers, except for the use of $^{13}C^{18}O_2$ in the gas fill.

I. Descriptions of Output Optics and Diagnostics

Figure 20 shows the layout of the output optics and diagnostics.

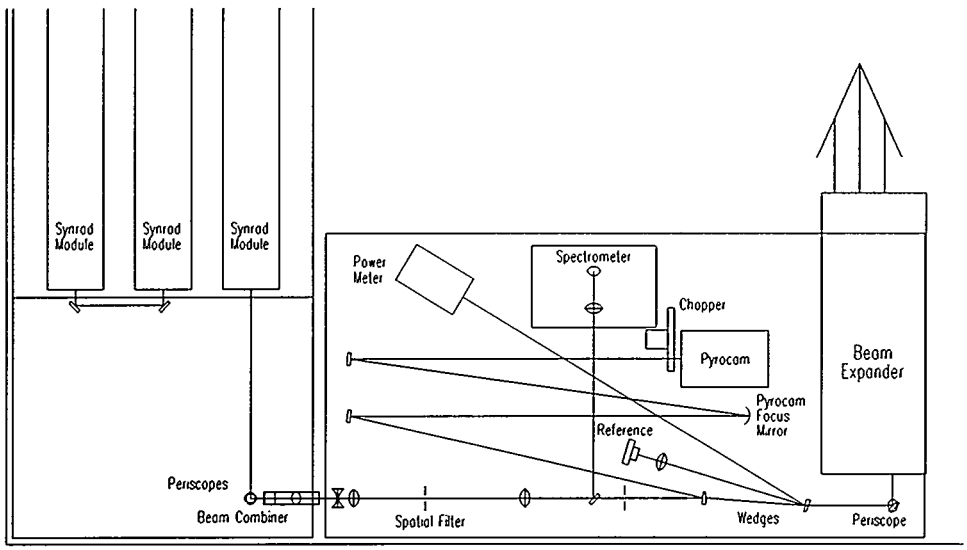

Figure 20. Layout of output optics and diagnostics

The final amplifiers of the two lasers are the two forward-most of the 6 modules. The two outputs are combined by the beam combiner, then spatially filtered. A removable mirror can be placed in the beam to direct the laser output to the spectrometer. A pair of AR-coated compensating wedges direct a small fraction of the light to the far-field monitor, the power meter, and the reference detector. Finally, the beam is expanded and directed to the final turn mirror mounted on the receiver secondary where the output is bore-sighted with the receiver.

J. Beam Combiner

The beam combiner, shown in Figure 21, consists of a periscope for each laser and a polarizing beam splitter used as a combiner.

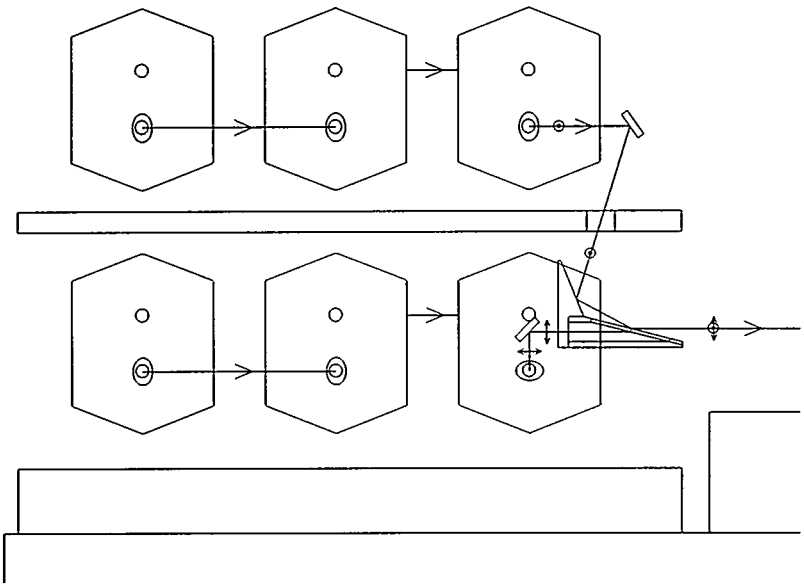

Figure 21. Details of the Beam Combiner

The $^{12}C^{16}O_2$ (normal) output from the lower laser (Laser 0) has its polarization flipped by a periscope (with two orthogonal 90° turns giving vertical polarization) followed by transmission through the beam combiner. The $^{13}C^{18}O_2$ output from the upper laser (Laser 1) has its horizontal polarization maintained through its periscope and is reflected by the combiner so as to be spatially overlapped and collinear with the $^{12}C^{16}O_2$ beam. The polarizer has a wavelength-dependent transmission of 95-98% for P-polarized light and a reflectivity of 92-95% for S-polarized light.

K. Spatial Filter

The spatial filter has two functions: to allow adjustment of the beam diameter and to filter the laser output to produce a nearly Gaussian beam. In order for the diagnostics to measure the outgoing beam as closely as possible, it is important that the limiting aperture be before the diagnostic beam splitting wedges. This is accomplished by locating the spatial filter pinhole at the input pupil for the remainder of the optical system. Since the final turn mirror at the receiver secondary is the normal limiting aperture, the entrance pupil has been positioned at the image of the final turn mirror. By sizing the pinhole appropriately, all light passing through the pinhole will reach both the diagnostics and the outside world without further vignetting. Due to the high gain and relatively large waveguide of the Synrad gain module, about 20% of the output is in high-order modes. These can be removed by the spatial filter, producing a nearly Gaussian beam. An adjustable focusing lens, formed by a negative lens followed by a positive lens (with a focus adjustment on the latter) gives adjustment of both the amount of spatial filtering and the diameter of the final transmitted beam.

L. Far-field Monitor

The far-field monitor consists of a Spiricon Pyrocam pyroelectric camera located at the focus of a spherical mirror. It provides a monitor of beam divergence and mode quality, overlap between the two lasers, and pointing variations. The Pyrocam has an active area of 12mm square and a pixel size of 0.1mm. The mirror focal length is 1.5m, giving an 18mrad square field of view and 150μrad resolution. The beam divergence at this point is about 3mrad. Light for this diagnostic comes from the first surface of the first diagnostic wedge, so that there is no chromatic aberration from the ZnSe wedge. The surface is AR-coated, giving a reflectivity at this angle of incidence of 0.5-1%, fairly independent of wavelength. Since pyroelectric detectors need a modulated light signal, the laser light is chopped by a New Focus Model 3501 chopper mounted immediately in front of the Pyrocam. The Pyrocam data is displayed on a VGA monitor, mounted at the DAC rack.

M. Power Meter

The power meter is a Scientech model MC2500 calorimeter, with a sensitivity of about 10μW. Fed from the AR-coated first surface reflection from the second diagnostic wedge, about 100mW should be incident on the meter. An analog readout is mounted on either the optical table or the DAC rack. This provides an absolute power measurement on the output of the lasers, giving a useful long-term diagnostic for laser performance, as well as an aid in laser alignment.

N. Reference Detector

The DIAL reference detector uses the reflection from the AR-coated second surface of the second diagnostic wedge. The detector, a Vigo System PC-L-2TE, thermal-electrically cooled (230°K) photoconductive HgCdTe detector, with a 1mm square active area, is at the focus of a 2" focal length lens. The spot size on the detector is ≈150μm, giving substantial leeway for reference-leg alignment variation without any significant effect on the reference reading. Likewise, while there is some dispersion in the focused position due to the diagnostic wedges, this is negligible compared to the size of the detector.

O. Spectrometer

A removable mirror on a kinematic mount allows the output of the lasers to be fed into an Optical Engineering spectrometer during laser alignment. The spectrometer is mounted vertically to reduce its footprint on the breadboard and make the observation screen easily accessible. The light is focused by a lens and then folded upward onto the slit.

P. Beam Expander

After passing through the diagnostic wedges, the beam is expanded with 10X magnification by a beam expander (Lambda/Ten Optics Model LBX100-10X). This is a Dall-Kirkham all-reflective design. The limiting clear aperture is that of the primary mirror with a diameter of 4.19". A periscope at the input to this device brings the beam to the height of the receiver and gimbal and also provides fine adjustment of the transmitted beam direction for centering it within the receiver field of view.

VI. Receiver

A. Introduction

The CACDI receiver design is based on the receiver subsystem developed for, and delivered to the second generation Tan Trailer during FY96. The subsystem includes a custom designed transimpedance amplifier with active baseline restoration circuits for 1/f noise rejection, and a pseudo matched filter for 100 ns pulses. The detector is a custom developed Mercury-Cadmium-Telluride (HgCdTe) semiconductor procured from Santa Barbra Research Center. Figure 22 shows an isometric view of the receiver subsystem, including the relay optics (discussed in section VII). The detector mounted on a sterling cycle mechanical cooler inside a dewar procured from Infrared Laboratories.

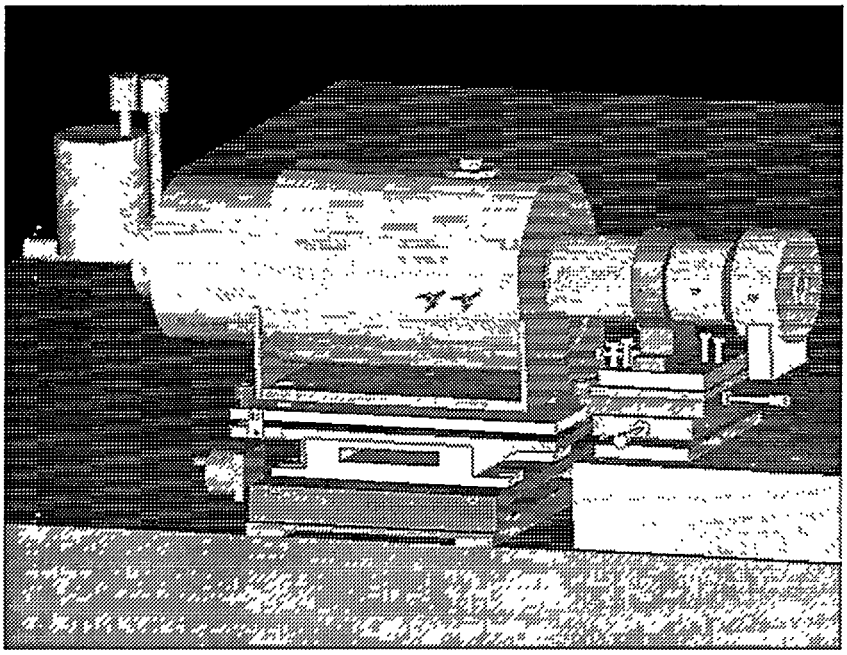

Figure 22. Isometric View of the CACDI Receiver and Relay Lens

B. Requirements

The receiver subsystem requirements are derived from the system level requirements presented in section III. Table 5 presents the requirements for the receiver subsystem.

Table 5. Receiver Subsystem Requirements

Requirement Description	Quantitative Value/Units
Detector Size	200 μm
Detector Electrical Bandwidth	20 MHz
Amplifier Electrical Bandwidth	10 MHz
Total Noise (NEP)	50 pW
Linear Dynamic Range	1000 to 1
Amplifier Gain	1,000,000 to 1
Telescope Aperture	30.5 cm (12 inches)
Effective f#	f1
Optical Bandwidth	8 -12 μm
Optical Throughput	0.65
Alignment	+ 5% of the Receiver FOV
Differential Mode Jitter	< 35 μradians

C. Detector

A set of detailed simulations of the DIAL lidar experiment were performed. From these runs, parameters such as optimal detector size, field of view of the receiver system, etc. were extracted. With this information, detector physics models were developed to obtain the required specifications. These derived specifications indicated that a substantial improvement over commercially available, off-the-shelf, amplifier and detector technologies would be required to obtain the goals for the subsystem. Tests were performed on a 100 micron square detector at cryogenic temperatures to verify this assumption. At 77°K the RoA, the detector impedance at 0 V bias, was 0.12 Ω cm^2 whereas at 30K the improvement was an RoA of 10 Ω cm^2. However, more importantly, the dynamic impedance (R_d), at 60 mV bias, changed from 4530 Ω at 77K to only 5917 Ω at 30K. Our models required an $R_d \geq 500{,}000$ Ω! Moreover, at 30K the leakage current under bias was 4.6 μamps whereas the model specification was 0.1 μamps! The results of this test and others indicated that an advanced detector was required. A suitable detector was identified from SBRC. These single element detectors were witness samples for a detector array

developed and used on another DOE project. Table 6 summarizes the comparison of the most pertinent detector specifications. Note the differences in the leakage current, RoA and dynamic impedance. The better performance comes from the details of the SBRC detector junction design. The one concession that was made in order to use these detectors was a requirement for cooling these devices from 77K down to around 35K in order to extend the long wavelength cutoff from 10.7 to 11.5 microns.

Table 6. Comparison of SBRC and Commercial Detectors. Note the leakage current, RoA and dynamic impedance values compared above. Note also the cutoff wavelength of the SBRC detector. To increase the cutoff out to 11.5 microns the detector was cooled below 35K.

Parameter	GEN II	Commercial Unit
	SBRC #2 V08	Kolmar 3090-1B
Size	200 μm square	100 μm square
Operating (Test) Temperature	77 K	77 K
Spectral Response (μm)	5-11	4 - 13
Cuton /off λ @77K (μm)	6 / 10.7	~9 / 12.4
Peak Response λ @77K (μm)	~9.5	~10
Quantum Eff. @9-11μm (%)	~85 (AR coated)	~50
Detector Bias (mV)	50	60
Leakage Current @ bias (μA)	<0.01	~5
RoA @77K	77	0.12
Dynamic Imped. (Ω @bias volt.)	5.75xE+6	4530

D. Amplifier

Before the detector was identified, it became clear that significant effort was required for the development of the receiver amplifier. The focus was on designing and building an amplifier with very low noise performance and high gain while maintaining the bandwidth required for 100 ns pulse detection.

When the breadboard amplifier was designed and built, it performed to within a few percent of the predictions. The subsequent prototype amplifier was fielded in the Generation II system. Table 7 summarizes the design features built into the LANL amplifier compared to the Kolmar amplifiers.

Table 7. Comparison of design features of the Kolmar and LANL amplifiers.

Parameter	GEN I Amplifier (10 MHz configuration)	GEN II Amplifier (80 ns configuration)
Transimpedance Gain (V/A)	10,000	1,000,000
Linear Dynamic Range	750 @ 10 kV/A gain	1000 @ 1 MV/A gain
1/f Noise Rejection	NO	DC to 200 Hz
DC Baseline Drift Control	NO	$< \pm 50\ \mu V$
Baseline Restore	NO	YES - 2 separate circuits
Active Bias Circuit	NO	holds bias to $< \pm 0.1$ mV (worst case)
Pseudo-Matched Filter	NO	YES

Some aspects of the GEN II design that are worth noting in detail include:

- The GEN I design incorporates a 2.5 kΩ feedback resistor whereas the Generation II amplifier has a 1MΩ feedback resistor. This yields a substantial decrease in the lower limit of the white noise floor of the Generation II amplifier with respect to the Generation I amplifier.
- The large 1MΩ feedback resistor, so desired for low noise operation, required the development of an integrator/derivative technique to maintain the appropriate frequency response.
- The pseudo-matched filter was set up to match a nominal pulse width of 80 ns (100ns with 20% margin). The gaussian laser pulse shape is approximated by a 5-pole filter to ensure a response which is a good representation of the gaussian pulse. Such a filter allows the minimum amount of noise contamination during pulse detection.
- An active bias control circuit holds the detector bias to at most ± 0.1mV. This minimizes 1/f drift of the detector and automatically compensates for background. A low pass filter in this circuit ensures that no bias adjustment will occur during laser pulse detection.
- A baseline restore circuit holds the current summing node of the first stage amplifier stable against 1/f amplifier drift to $< \pm 50\ \mu V$.
- A similar baseline restore circuit holds the voltage summing node of the pseudo-matched filter against 1/f drift to $< \pm 50\ \mu V$.

Modifications incorporated from the basic Generation II receiver amplifier include the incorporation of a buffer amplifier at the output of the 1,000,000 to 1 gain amplifier. This stage is provided to isolate the main amplifier from the impedance of the long cable between the receiver and the DAC. The second modification was the addition of a 400 Hz notch filter at the input to the DAC to reject 400 Hz noise picked up on the same cable.

Low noise operation is further enhanced by utilizing a battery power supply. Utilizing battery power isolates the sensitive circuitry from typical power line voltage fluctuations. The batteries are recharged

utilizing a standard charging system powered by the aircraft 110V, 60 Hz, ac power line. Power for the charger is obtained from the power distribution box on the Optic Assembly Table. Charging is performed prior to pre-flight checkout. Typically, the batteries have 18 hours of useful life before re-charging is required.

E. Mechanical Cooler

A mechanical cooler has replaced the two stage liquid helium/liquid nitrogen dewar utilized on the Generation II receiver. This was done because of the limited life-time on the order of 6 hours, and the difficulty of working with liquid helium within the confined spaces aboard the Argus aircraft.

The mechanical cooler provides liquid helium temperatures to the cold head. Temperature control provided by the cooler allows the detector head to be set at 25°K for normal operation. A cold filter wheel mounted internal to the cooler provides five positions for three specific bandpass optical filters, a blank, and an open port. The cold filter is maintained at 77°K. The blank position and the open position are used during subsystem performance verification testing. The three bandpass filters are utilized during field operations. The bandpass specifications are 8.5 - 11.4mm , 8.75 - 11.75mm, 9 - 17mm.

In order to match the $f1$ optical design of the receiver the mechanical cooler provides a 60° FOV. Further, a fine focus adjustment is provided to allow for changes in the received beam focus due to temperature fluctuations. Finally, the aperture window of the cooler is AR coated to provide maximum throughput.

The cooler is driven by a compressor located on the aft laser support pallet. This compressor interfaces with the cooler through a 1.25 inch O.D. bellows tube that is covered by a stainless steel mesh. The compressor hose runs at 245 - 270 psig. Two hoses are used. The first runs from the compressor to a interface connector mounted off the Optic Assembly Table. This first hose is 300 inches long. The second, 72 inches, long run from the interface connector to the expander. The interface connector provides vibration dampening from compressor vibrations. The compressor is powered by the Argus 208V, 60 Hz, 3 phase, Belhman power supply. The compressor provides electrical power to the cold head expander. A clam shell cover is supplied by Infrared Labs to contain the bellows in the event of a crash. This shell ensures that the mechanical cooler meets the 9 g forward load crash requirement.

Pre-cooling of the mechanical cooler is required to reduce the time needed to bring the cold head from ambient temperature down to 25°K. This is done by supplying liquid nitrogen to the cooler to bring the system to 77°K. The pre-cool must be performed 3.5 hours before pre-flight checkout. After three hours of pre-cooling the compressor is turned on and will bring the cold head to temperature in 30 minutes.

VII. Data Acquisition and Control

A. Introduction

The CACDI data acquisition and control (DAC) system is an evolution of both the CALIOPE Tan Trailer, Generation II and the N-ABLE DAC systems. The primary new requirements which drive the CACDI DAC design include:

- Laser wavelength tuning rates to 5 kHz: This is the single most significant requirement impacting the design of the CACDI DAC. The Generation II system supported galvanometer tuning with maximum tuning rates to 150 Hz. Tuning was accomplished under software control in the real-time control processor. For CACDI, in order to support tuning at 5 kHz for each laser, a completely new timing system has been designed in which all of the necessary parameters for both lasers and tuners, for each desired wavelength, can be pre-loaded into a memory. Clocked hardware then converts these parameters into the necessary timing and level control signals in sequence at the required rates.

- Automatic range-to-target correction: Knowledge of the range-to-target is required in order to set the delay values for triggering the boxcar integrator gates which control the integration window for the receiver signals. N-ABLE provided for automatic ranging in either of two modes. a) GPS data obtained from the Argus data broadcast could alternatively be used to auto-adjust the boxcar gate delay at the GPS update rate of once per second. While this scheme provided marginally satisfactory results for N-ABLE, it does not have sufficient accuracy for the higher precision gating required for the 200 to 400 ns pulse-widths associated with the CACDI lasers. b) Waveform auto-ranging allowed for calculation of the receiver boxcar gate delay based on the time the receiver signal, recorded with a waveform digitizer, crossed a selectable threshold. While providing excellent performance in high signal-to-noise applications, this technique was unusable at longer ranges where signal-to-noise ratios fell below two. For CACDI this approach will be extended by incorporating a waveform averaging algorithm in high-speed reconfigurable logic. A running average of the last n waveforms will be maintained in hardware in order to improve the signal-to-noise and allow range-to-target determination at CACDI ranges of interest with sufficiently high update rates to maintain boxcar gating to the required accuracy of < 10m (67ns). A more detailed explanation is given under System Description below.

- Laser pulse repetition rates to 5 kHz: At the 2 kHz pulse repetition rates of the Generation II DAC there were certain operational circumstances during which the performance of the DAC was marginal. A higher performance DAC will be required for the higher CACDI data rates.

- Real-time processing during acquisition: It appears to be increasingly important to be able to perform certain algorithms in real-time as the data is being acquired. Such processing, although not yet specified in detail, might include binning the data by wavelength, averaging the data by wavelength, and performing limited chemometric calculations on the data as it is being acquired. In this way greatly reduced sets of pre-processed data could be sent to the analysis machines for faster chemometric analysis and interactive optimization of the wavelengths being used in the experiment.

B. Approach

As discussed above, new hardware is in the final stages of development to meet requirements. This hardware will be implemented along with the CACDI laser system during the initial integration phase. The reconfigurable logic hardware discussed above is in the early stages of development and will be demonstrated and then integrated during the field-testing phase of CACDI. In order to meet the demands imposed by higher data rates several hardware enhancements to the Generation II system have been implemented for CACDI. These include faster processors for data acquisition, and analysis; faster networking hardware; and faster disks for data archiving. These will be discussed under System Description below. The final system enhancement, a data server, is discussed under Data Storage and Distribution.

C. System Description

The heart of the DAC, shown in Figure 23, BD-1, is the I/O controller (IOC). This is a Motorola 200 MHz, MVME-2604 PowerPC processor running the VxWorks real-time operating system. Benchmarks of this processor indicate about a factor of 20 performance improvement over the 68040 processors used in previous systems. The 2604 is the system controller in a 21-slot VME chassis. It orchestrates the operation of a number of VME I/O modules, responding to various interrupts and gathering data as required. It may perform some minimal preliminary analysis on data before sending it off over a network connection to the operator's workstation or the analysis workstation.

The timing module is an Industry Pack (IP) carrier module which holds two custom IP boards containing Field Programmable Gate Arrays (FPGAs) and memory. The timing module provides all of the signals necessary to control the lasers, AO tuners, AO modulators, boxcar integrators, A/D converters, and transient recorder. All of the parameters necessary to specify a given pattern or patterns of wavelength sequences for both lasers are loaded into the memory of the timing module. Driven by an on-board oscillator these parameters are then converted to provide the necessary timing and control signals at the specified rate.

Signals generated in the timing module are carried on ribbon cable to the signal interface (SI) chassis where they are buffered and broken out onto the various connector/cable combinations as required. The SI chassis also serves as a convenient location to monitor all signals with a scope for diagnostic purposes. In addition, the SI chassis performs a ground-isolation function. All control lines to the laser support racks are optically coupled to avoid the necessity of tying the laser support rack ground to the DAC racks. Similarly, differential buffers are used on the transmit and receive signals from the optical table to minimize ground loops.

Six EG&G Model 4121B boxcar integrators are used for measuring the energy from the transmit and receive pulses. The output of the transmitter pulse monitor is input to a threshold comparator in order to derive the optical trigger pulses which are used as the time references to which all boxcar triggers are derived. To account for the delay in the comparator and trigger circuitry and to provide for triggering the boxcars in advance of the signals they will integrate, a cable delay line will be inserted in the signal path to boxcars 0 and 1. There is a possibility that back scatter off the Argus window will momentarily saturate the receiver, resulting in the return signal being superimposed on a baseline that is slowly recovering to its steady state level. Such a sloping baseline would introduce an error in the integration of the receive signals. Therefore, two additional boxcars will be used to measure the baseline level immediately prior to the first laser return and after the second laser return. Boxcars 2 and 3 will be triggered approximately 2 μs before the anticipated laser0 return and boxcars 4 and 5 will be triggered approximately 50 ns before the anticipated laser1 return. Boxcars 3 and 5 will have 2 μs delays dialed into their internal delay circuits, while the internal delays for boxcars 0, 1, 2, and 4 will be set to 0.

The analog-to-digital converter modules designated A/D0 and A/D1 are model VMIVME-3114A from VMIC. Each module has four differential inputs with simultaneous sample and hold circuitry. A/D0 will be triggered to sample and digitize the outputs of boxcars 0 and 1 after the last-sample-valid (LSV) signal from both boxcar1 has been asserted. Similarly, A/D1 will be triggered to sample and digitize the outputs of boxcars 2, 3, 4 and 5 after the last-sample-valid (LSV) signal from boxcar5 has been asserted.

In order to accurately trigger the receive boxcars at the appropriate times, the range-to-target distance must be accurately known. Experience from the N-ABLE experiment indicates that when flying circular orbits around a target, the Argus range-to-target rate of change can vary due to cross-winds and other factors by as much as 30 m/s. N-ABLE employed a simple scheme whereby the point at which the digitized return waveform crossed a threshold level was used to calculate the range-to-target and thereby set boxcar trigger times. This scheme worked well for close range experiments where signal-to-noise was high, but was unsatisfactory for longer ranges. For CACDI, this scheme will be extended. A transient recorder will digitize the return signal from each pulse of the desired laser. A running average of n waveforms will be computed using a reconfigurable logic module with the averaging algorithm

implemented in FPGA hardware. The peak of the running average will be determined by the hardware, thus providing a measure of the range-to-target.

Figure 24, BD-2 illustrates the details of receiver gain selection. A coaxial-relay signal selector switch mounted on the outside of the receiver enclosure will allow the operator to optionally multiply the nominal gain by 10x or 100x to the nominal receiver gain. A programmable coaxial attenuator will provide for intermediate values as desired. These switches require 28VDC control voltages which will be supplied from the Argus 28VDC bus and switched through a VMIVME-2120-175N binary output module. Hardware and software identical to that used on N-ABLE will be implemented for this function.

The receiver filter wheel will be identical to the one used on N-ABLE. On N-ABLE the filter wheel control box was mounted on the receiver enclosure and its control connector was replaced with a military circular style. For CACDI the location of the control box and connector details are still TBD. Figure 24, BD-2 reflects the control scheme used for N-ABLE incorporating a VMIVME-2120-280N binary output module.

Figure 25, BD-3 indicates the connection to the Argus IRIG-B time reference. This connection is made using RG316/U coaxial cable to a Datum Model BC336VME timing module in the DAC VME chassis. All data time-stamps are generated by reading this module.

The IOC processor will communicate data to the operator and analysis workstations through the ethernet hub shown in Figure 25, BD-3. The interconnecting cables will be 100BaseTX shielded cables with RJ-45 connectors on each end. This network potentially offers a speed improvement of an order of magnitude over those used for N-ABLE and Generation II. A transceiver to allow a BNC connection to the 10Base2 Argus network will be provided so that the Argus broadcast data packets may be received and archived along with the other CACDI data sets.

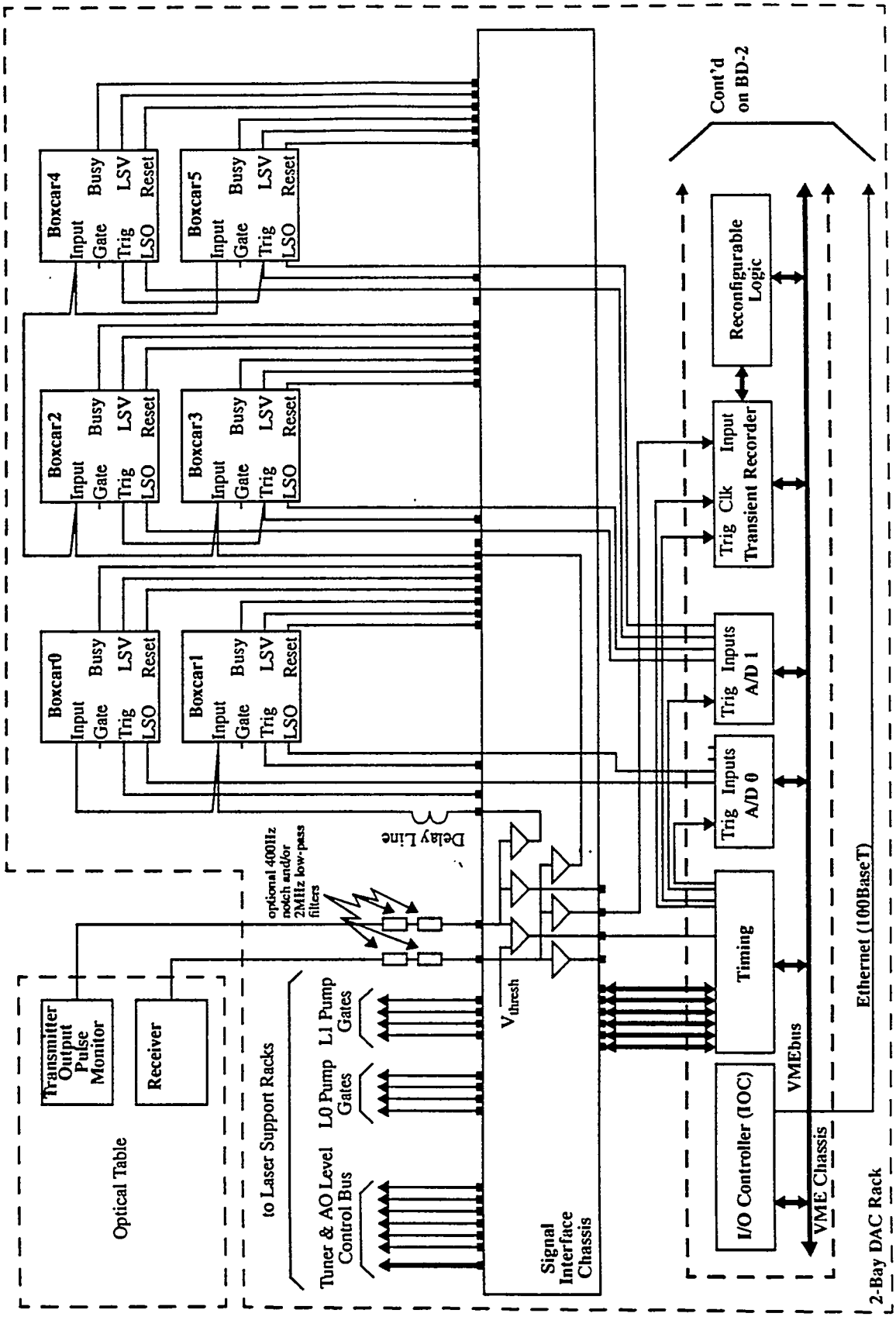

Figure 24. CACDI Data Acquisition and Control Subsystem Block Diagram, BD-1

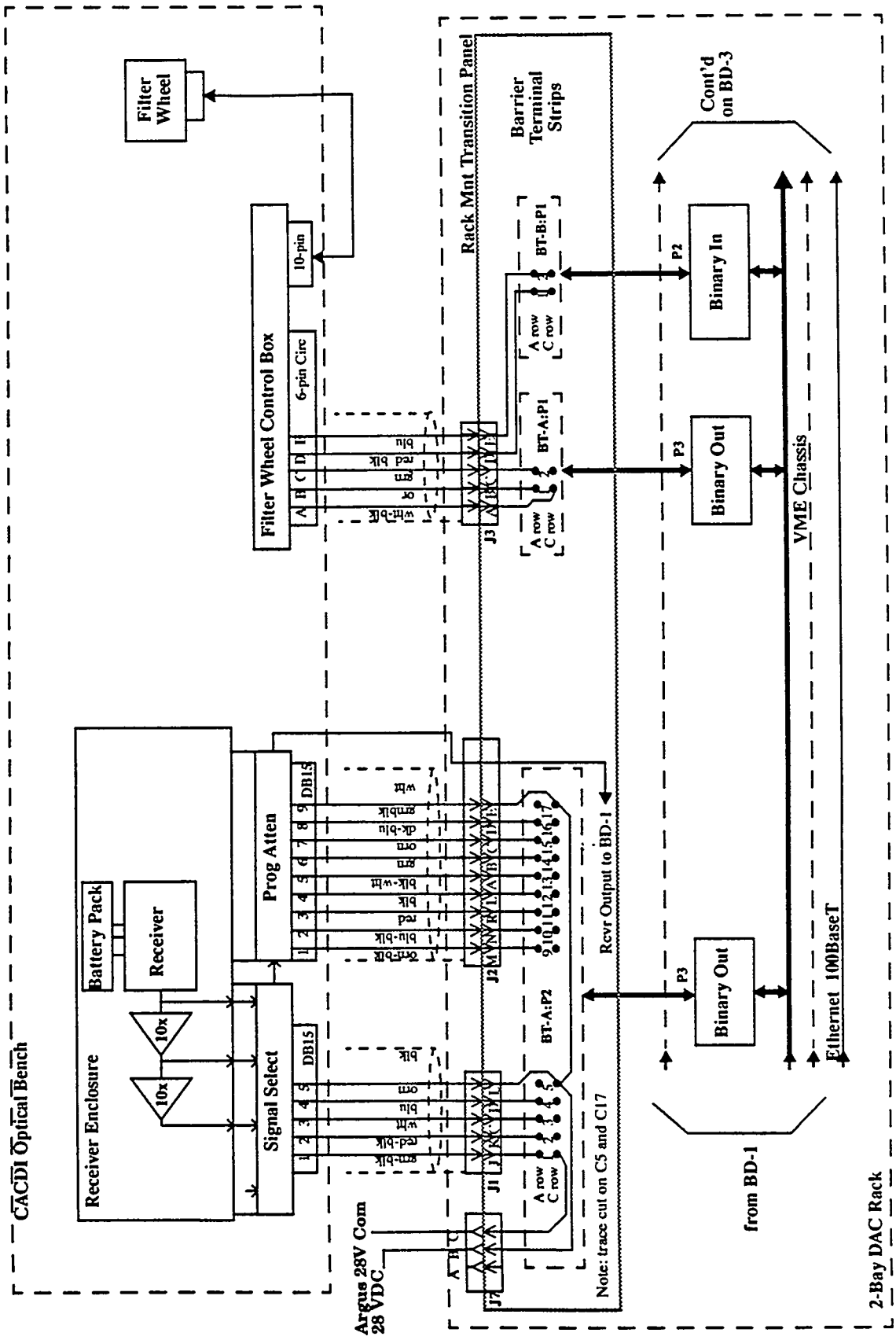

Figure 25. CACDI Data Acquisition and Control System Block Diagram, BD-2

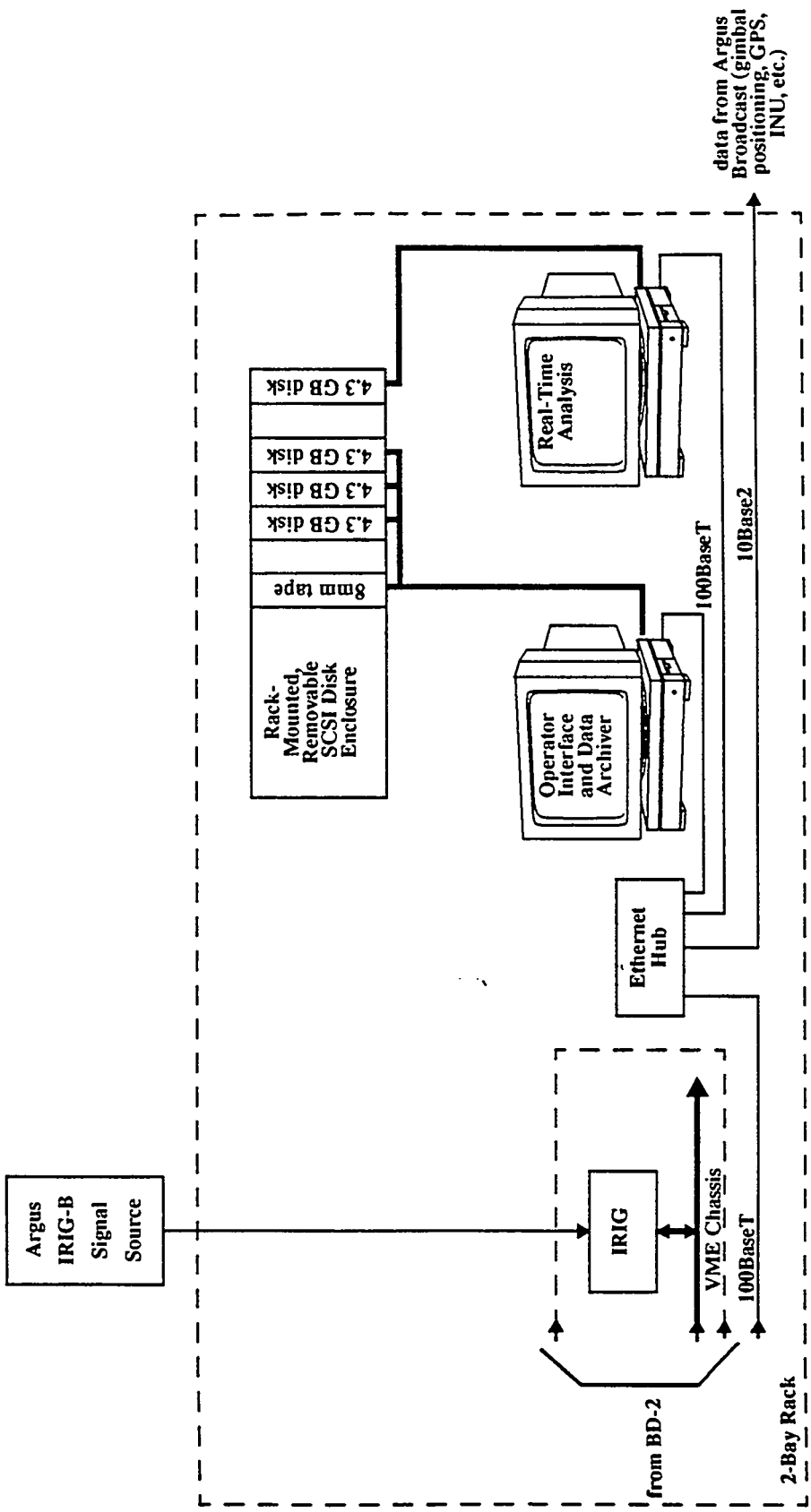

Figure 26. CACDI Data Acquisition and Control Subsystem Block Diagram, BD-3

The operator will control the experiment utilizing a number of graphical user interfaces (GUIs) from the operator workstation. These displays will enable him to control the lasers and assess their performance. In addition he will be able to control receiver gain, filter wheel position, and data archiving. A number of displays will enable him to view other important experimental parameters including averaged return signal waveforms. The workstation will also perform the function of archiving data to disk. For CACDI this workstation will be an ultraSPARC 170E with a performance increase of about eight over the SPARC-20 used in the N-ABLE and Generation II DACs. The fast-wide SCSI bus and disks on the ultraSPARC yield a factor to two improvement in data access and storage times over previous DACs.

The analysis workstation will be used by a second experimenter to analyze data and assess the success of the experiment. This activity will include a comprehensive C-based analysis tools specifically written for CACDI. As backup, the "Real-Time MATLAB Tool", which has been used quite successfully on the N-ABLE and Generation II systems, will be available. Both schemes allow opening TCP/IP socket connections providing a data stream between the IOC which is collecting the data and the analysis workstation. Each instance of this tool opens another data socket connection which the IOC attempts to service with the data requested. This workstation will be an ultraSPARC 170E with a performance increase of about eight over the SPARC-20 used in the N-ABLE and Generation DACs.

D. Data Storage and Real-Time Data Distribution

At the pulse repetition rates of Generation I and N-ABLE (<100 Hz) distributing data to various requestors from the data source, the IOC, was the simplest and most logical implementation. Excellent performance was achieved for the data rates of these early systems. However, with the advent of Generation II, data rates increased by more than a factor of 20. In addition, at NTS during June of '95 it was not uncommon to have three and sometimes four workstations requesting data from the IOC in real-time. Under such conditions it was possible to saturate the IOC with data distribution tasks. It became clear that moving the data distribution task from the IOC, which must handle the data in a deterministic manner, to a dedicated data server node would be a worthwhile design improvement. In this design, the IOC would pass one copy of the data to the data server which would then handle the task of archiving and distributing the data to other requesting nodes in a prioritized manner. This approach, however, requires a rather significant design effort. With the enhanced performance of the CACDI processors, the existing design is not expected to be a problem

VIII. Receiver Optics and Alignment

The receiver and alignment optical design is shown in Figure 27. The subsystem accommodates two visible acquisition cameras, that support the Argus pointing and tracking subsystem, the CACDI receiver, and the CACDI system alignment hardware. The transmitter and receiver of the CACDI design become coaxial by

folding the transmitter beam off a mirror mounted on the rear of the receiver telescope secondary mirror. The Argus Pointing/Tracking Mirror (PTM) directs both the transmit beam and receiver FOV to the desired target on the ground.

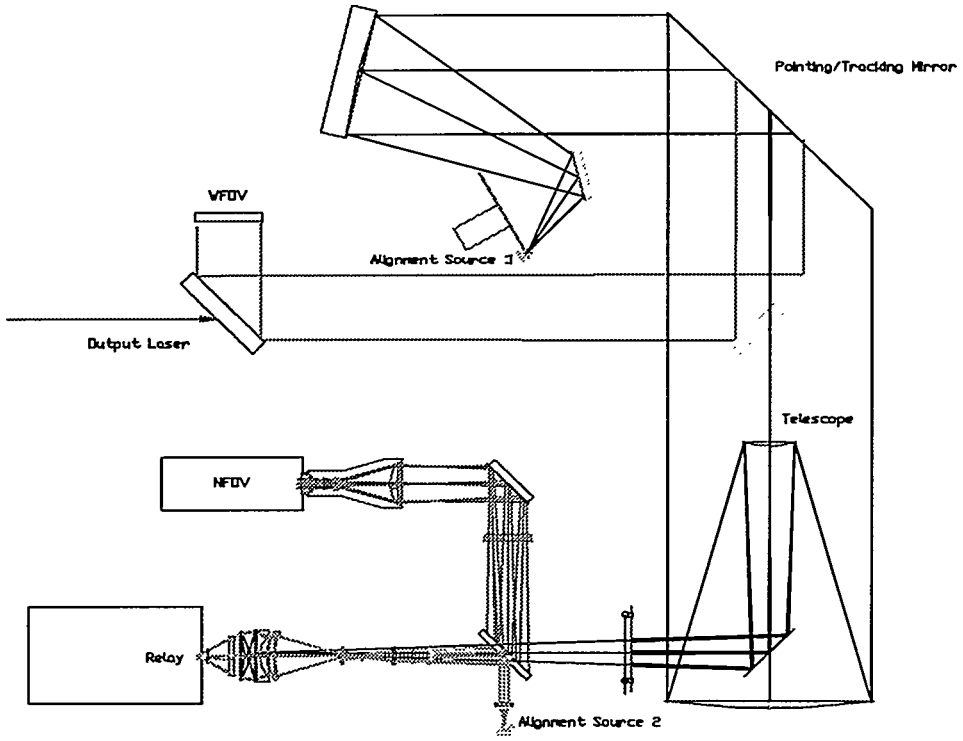

Figure 26. CACDI Receiver and Alignment Optical Design

A. Receiver Optics

The relay optics for the CACDI receiver subsystem are designed to allow for imaging of a 13.3m spot on the ground at a distance of 20 km onto a 200 micron detector with correction over the 8-12 micron wavelength bands. Edge definition of the ground spot is assured by creating a good quality image on the detector plane. The relay optical design allows placement of various Neutral Density (ND) filters into the infrared beam path without degradation of the imaging position at the focal plane. Stray light has also been minimized to first order to keep spurious signals from entering the detector plane area. Finally, the receiver optical design allows for splitting off a visible beam (0.6 - 0.9 μm) for the Narrow Field of View (NFOV) imaging acquisition camera.

The receiver relay optics are composed of seven lenses placed near the focus of an f/14.66 centrally-obscured 12 inch diameter telescope. The NFOV splitter is placed into the beam before it arrives at the relay optics' first element. The first element collimates the incoming light to allow for placement of various ND filters via a five position computer controlled filter wheel. The beam at this point is about

20mm in diameter. Once through the collimated region, the light is focused by another lens to eliminate secondary reflections from the NFOV beam splitter as well as other ghosts generated by the first two forward-optics. A single field lens reshapes the divergent light for final manipulation by the last four lenses, one of which is a Germanium (Ge) lens element used for color correction across the wavelength band. The design requires a 60 degree full field-of-view (FFOV) into the detector through a ZnSe window as well as a Ge cold filter.

The relay assembly was re-optimized after completion of final lens fabrication, coating, and optical measurement by the manufacturer. This allowed for the lens elements to be dropped into the relay mechanical housing without further adjustment. The bare design, after re-optimization, prior to fabrication, had a 0.075 rms wavefront error (wavelength = 9.1 microns) on-axis and 0.11 rms wavefront error at the extreme field. Diffraction point-spread function analysis shows that edge definition of the ground spot should be on the order of 0.5 meter. The possible misalignments expected could result in a doubling of these wavefront degradations. The mechanical barrel is made from aluminum. The coatings on the lenses, splitters, and mirrors (including the central obscuration) allow for approximately 77-88% throughput before entering the detector package.

B. WFOV Imaging Camera

The Wide Field of View (WFOV) optical relay is the same device used on the N-ABLE system. It is provided by PL/LIMF. The narrowest FOV attainable by the WFOV relay system is 2.5 degrees (436 meters on the ground from 10 km), with a zoom capability of 16:1. The WFOV beam splitter allows the LOS for the four inch diameter lens assembly to follow the path of the laser output to the ground scene. The camera is the same as that described in the NFOV optical train. A corrector wedge is placed between the beam splitter and the WFOV lens relay to correct for effects of the aircraft window. This optic has the same wedge as the window and is also made of ZnSe, although only 10 mm thick. The 7 inch diameter beam splitter passes the laser transmitter output beam but reflects the 0.6 -0.9 μm WFOV sensing illumination.

C. NFOV Imaging Lenses

The NFOV lens assembly is composed of 6 elements positioned to collect the light reflected from the dichroic beam-splitter. The lens assembly images a 120m spot on the ground at 10km onto a 12mm detector. Analysis shows that the initial design has sub-pixel diffraction point-spread image quality with resolving power on the ground on the order of 5cm. Ghost images may be a problem on the detector, if the AR coatings on the lenses do not meet specification. A small wedge is placed in the converging telescope beam to correct for the chromatic effects of the large wedged window in the aircraft. The lens

assembly is corrected for this effect over the wavelength range of 0.6-0.9 microns, where the intensified camera is most sensitive.

D. Alignment Optics

The alignment of the CACDI system optical train; telescope, dichroic beam splitter, relay lens assembly, laser, and detector can be monitored using two separate pinhole blackbody assemblies. The first of the two assemblies reflects light into the receiver optical path using the NFOV dichroic beam splitter. Beam shaping of the blackbody signal is performed using a single lens. This allows for monitoring of the position of the detector relative to the relay without the effects of the telescope.

An off-axis parabola sends a collimated beam from the second blackbody, located in the middle of the Optic Assembly Bench, into the front of the telescope. The laser is aligned to the same pinhole, using a fold flat mounted directly behind the telescope secondary mirror, and monitored using the NFOV camera. Precise adjustments of the pointing/tracking mirror are required for repeatable placement of this fold flat, which directs the line of sight into the telescope.

IX. Ground Support Equipment

A. Introduction

Two areas of ground support are required to meet the programmatic goals of the CACDI field experiments described in Section X. This includes the support required for ground-based experiments, and that required for airborne experiments. Much of the support equipment is the same for both aspects of the field experimental plan. However, there are unique requirements for each. Ground support will vary, depending on the field location of the experiments; e.g., Los Alamos, Nevada Test Site, etc. The major ground support activities, logistics and equipment that are required to complete the CACDI field mission are discussed below.

B. Airborne operations

The Phillips Laboratory Argus aircraft will be used for CACDI airborne operations. The aircraft is a C-135 airframe modified for use as an airborne electro-optical laboratory (Figure 27). A port side optical window, in the forward section of the aircraft, allows the LIDAR laser beam to propagate from the aircraft toward the ground DIAL target.

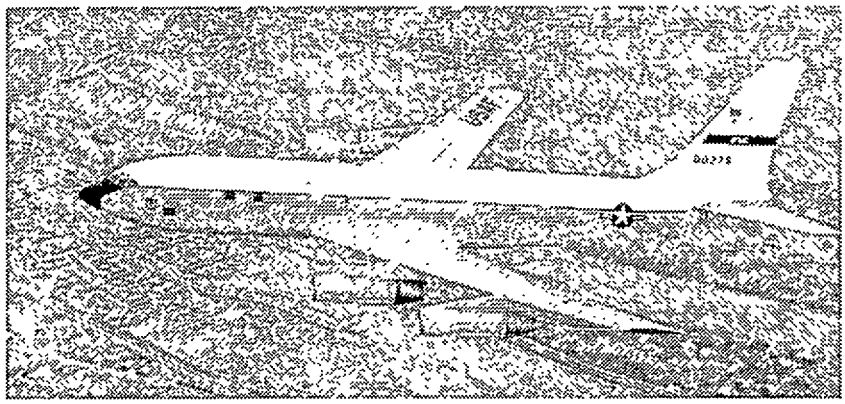

Figure 27. Argus Aircraft

The aircraft will be flown in orbits around the DIAL target area, at a slant angle of 20 degrees. The slant range to the target will be between 7.5 and 20 km. Figure 28 shows pictorially, the preferred flight scenario. The orbit duration is dictated by the set of experiments being conducted during a particular flight. N-ABLE experience shows that arial missions lasting three to four hours can be anticipated. At this time it is planned that all experimental flights will occur during daylight hours. However, contingency plans are in place, should experimental needs or other factors require night time operation. These contingencies are discussed later in the "Pointing Targets" section of this report.

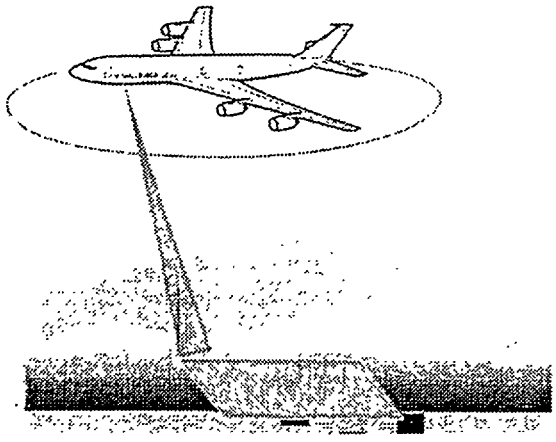

PREFERRED FLIGHT SCENARIO

C-135 Aircraft
Daytime flights
Slant angle: 20 degrees
Slant range: 7.5 to 20 km
Flight duration: 2 to 3 hours at DIAL target
Flight Frequency: 2 or 3 flights per week

Figure 28. Preferred Flight Scenario

CACDI airborne experiments are slated for three locations; Los Alamos, Nevada Test Site (NTS) and one additional site, yet to be determined. The schedule for these airborne intensive periods (AIPs) is listed in Table 8. During AIPs, experimental flights will be scheduled at a maximum of every other day, with two or three flights per week, weather permitting. N-ABLE experience demonstrates that this is an appropriate schedule to allow for crew rest, data analysis, mission planning, equipment maintenance, etc.

Table 8. Airborne Intensive Periods

AIP Location	Date
Los Alamos	November 1997
Nevada Test Site RSTR	June 1 - 18, 1998
Additional Site (TBD)	TBD

C. Aircraft Staging for Airborne Intensive Periods

During CACDI system integration into the Argus aircraft (in preparation for airborne campaigns), the Argus aircraft will be staged at pad 14, Kirtland AFB, Albuquerque, NM. It will be used as the staging base for the Los Alamos area AIP, as well. System alignment, benchmark testing and fundamental optimization will be conducted prior to commencement of airborne operations. Both internal and external laser operations are required for these ground-based tests. The Philips Laboratory outdoor laser range, adjacent to the Argus ramp, will be used for external, far field (down range) laser operations.

During the NTS AIP, the Argus aircraft will be staged at the DOE Remote Sensing Lab (RSL) located at Nellis AFB, Las Vegas, NV. External laser operation is required for laser/receiver alignment and related pre-flight tasks. Vacant Nellis AFB property, adjacent to the RSL ramp, will be used for this purpose. An exclusion zone will be determined and marked, to ensure personnel safety.

D. Tan Trailer Generation II support of Airborne Operations during AIPs

The Tan Trailer, Generation II will be used during CACDI AIPs conducted at Los Alamos and at NTS for ground-truth of airborne measurements. This may include incorporation of the IR camera into the Tan Trailer receiver system for in-situ plume tracking and DIAL measurements. During Los Alamos operations, Tan Trailer, Generation II will be positioned at its normal field location at TA-33. It will be turned 180 degrees from its normal pointing direction to facilitate probing the same DIAL scene that the airborne system will be interrogating.

During NTS AIP, Tan Trailer, Generation II will be positioned at the 20 km pad (Monastery, Figure 29). Interrogation of the RSTR DIAL scene from this location has been accomplished in two previous missions; procedures for CACDI will be similar to those used in the past.

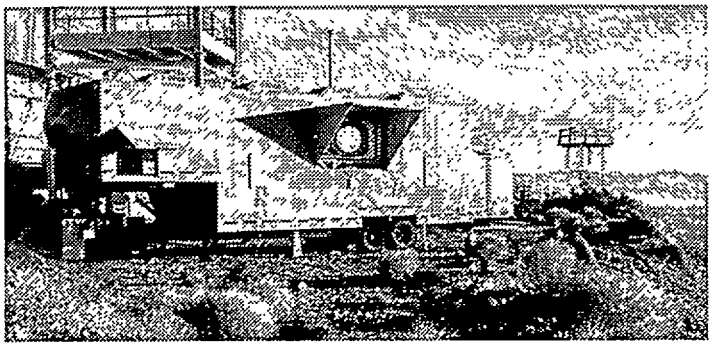

Figure 29. Tan Trailer at Nevada Test Site, Monastery

E. Targets for Airborne Experiments

Two types of targets are required for airborne DIAL experiments; lidar targets and pointing targets. Lidar targets are those directly related to DIAL return signals. Pointing targets are those required to confirm optical alignment of the airborne CACDI subsystems and maintain pointing at the lidar target in the presence of aircraft motion.

1. Lidar Targets for NTS Experiments

For airborne chemical plume interrogation at NTS, only natural targets will be used. At NTS the indigenous albedo is primarily dry lake bed, with a man-made gravel area coming into view for short periods of time, during each orbit.

Calibrated targets will be used to aid in atmospheric and related statistical measurements. The calibrated target material for airborne experiments is yet to be determined. Field experiments will be conducted at Los Alamos, over the next several months, to find a suitable material. The leading candidate is aluminum screen. The target will be 120 feet in diameter placed horizontally on an open area of the lake bed. This will provide an unobstructed view for the CACDI system onboard the Argus aircraft.

Existing calibrated targets will be used for the ground-based, support experiments (Tan Trailer, Generation II) at NTS. One of the elevated, 12' by 12' target backstops will be used and positioned as required behind the wind tunnel or stack, in line with the chemical plume. LANL will furnish the sand-blasted aluminum sheets for mounting on the backstops. The feasibility of using the 40' by 40' NTS target at this point is questionable. Given its fixed location and its current condition, it may not be cost effective to use this target. The CALIOPE Field Team will assess the need for this target, based on experimental requirements, within the next several months.

2. LIDAR Targets for Los Alamos Experiments

An open, relatively flat, area at TA-33 is under consideration as the target region for local airborne DIAL experiments. The area is large enough to have a natural (dirt & short foliage) target in close proximity to a calibrated target. Either target can be used, with or without chemical plume, as experimental need dictates. As stated earlier, the calibrated target material is yet to be determined.

A vertical, 12' by 12' sand blasted aluminum target will be positioned for Tan Trailer, Generation II viewing of the DIAL scene as required by the experimental plan. Natural targets in the TA-33 area will also be used for this purpose.

3. Pointing Targets

A "high-contrast' target is required for Argus pointing and tracking during daylight operation. The target will consist of painted, 4' by 8' plywood sheets, some flat white, some flat-black, that will be laid on the ground in the appropriate pattern to provide for accurate lock-on and tracking. For the case of the NTS lake bed, the sheets can be "nailed" right into the lake bed. For uneven areas at Los Alamos, a flat, rigid frame will be constructed. Based on N-ABLE experience, this design will be adequate. To insure that this is the case, we will provide Phillips Lab with a similar target for trial operations during upcoming LARS flights (scheduled September, 1997) to confirm acceptable locking, pointing and tracking.

Currently, the plan is to have all daytime (daylight) experimental flights eliminating the need for tracking and pointing beacons. However, in the event night time flights are required, the same beacon/strobe design (successfully employed during the N-ABLE program) will be used.

Two procedures are under consideration to confirm airborne optical system alignment. The first uses the edges of the "calibrated" lidar target to demonstrate predicted return signal variations as the laser beam is moved on and off the target. The second, uses a small corner cube to demonstrate signal return variation as predicted. Both procedures will be tried during Los Alamos airborne experiments to determine the preferred method for the following operations at NTS.

F. AIP Communications (voice and IR camera telemetry)

During AIPs, efficient communication among the CACDI aircrew, the CACDI ground support teams, and the chemical release team will be required to effectively execute airborne experiments. A teleconference or video conference system will be used to facilitate pre- and post-flight briefings between these teams. For example, during the NTS AIP, team members assigned to NTS will assemble at the video conference center at Mercury and team members assigned to the Argus aircraft will assemble at the RSL video conference room to discuss daily flight activities. A telephone voice messaging system will be employed

for daily updates and schedules. Any interested individual will be able to call the appropriate number and receive flight schedule information. A cellular phone will be available aboard the Argus aircraft. This phone will be used by flight crew members to communicate with NTS facilities while Argus is on the ground. This will be the only remote communication link to the Argus aircraft while on the ground. The cellular phone must be turned off during airborne operations, per USAF regulations.

Once airborne, communication between the aircraft and the ground shifts to UHF radio (LOS) communication, supplied by the USAF. Figure 30 depicts the general communication architecture that will be used during airborne operations. To minimize confusion, a single UHF frequency is used as the link between the Aircraft Coordinator and the Ground Coordinator. Only these two individuals communicate between the ground and aircraft. Communications from all other personnel or teams is through the appropriate coordinator, both aboard the aircraft and on the ground. "Receive only" radios will be available for those who need to hear the air-to-ground conversations. Telephones and/or VHF radios will be used for communications between ground teams and the Ground Coordinator. The Argus aircraft has a built in communications network that affords this capability for personnel aboard the aircraft.

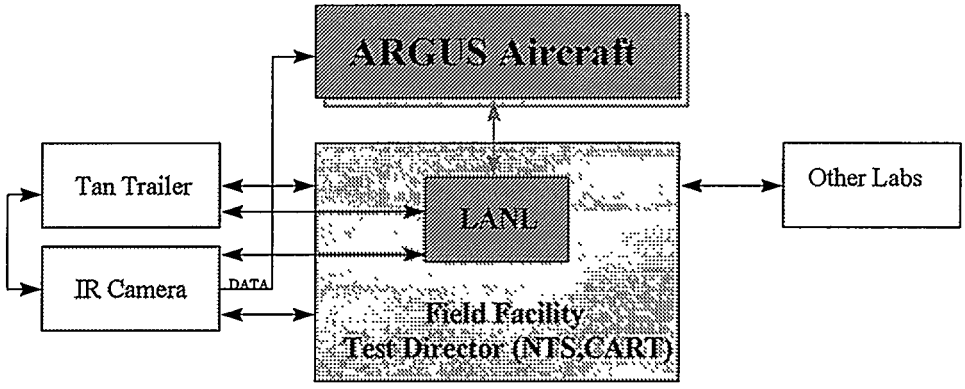

Figure 30. AIP Communication Architecture

Telemetry of the ground-based IR camera data to the aircraft is accomplished using spread-spectrum VHF radio transceivers, at power levels below FAA regulation. The video image of the target scene will be transmitted to the aircraft. Radio frequency approvals will be obtained from appropriate LANL and NTS officials.

G. Data Security

The data security plan for airborne operations is under development. DOD, as well as DOE requirements are being considered and will be included in the resultant plan. To facilitate post-flight data analysis during the NTS campaign, room at the Remote Sensing Lab (a "Q" level facility), Nellis AFB, is being

requested for classified computing. Space for four computers and as many personnel is required. Likewise, similar facilities are being sought at Nevada Test Site, RSTR area, and Kirtland AFB, as needs dictate.

H. Passive Imaging

The infrared passive imager is a 256 pixel by 256 pixel HgCdTe detector focal plane array camera. It will be used for all airborne operations for a two-fold purpose. First, it will assist in laser beam pointing and quality measurements. Secondly, it will assist in plume verification.

For airborne experiments at Los Alamos, it will be positioned atop building 209 at TA-33. The building is approximately 50 feet tall and has a clear view of the DIAL target area.

For airborne experiments at the NTS, it will be secured on a scissors lift and raised into position prior to testing. The scissors lift will be positioned somewhere near the DIAL target area on the lake bed. The exact location and height are yet to be determined. Because of strong winds, the lift will need to be guyed, at its raised height.

The camera will be remotely operable through radio control. Data will be transmitted, via radio, to a control point - located in building 39, TA-33, for Los Alamos experiments and in the RSTR Control building during the NTS flight campaign. The data will be relayed from there to the aircraft. Radio frequency authorization will be obtained from the appropriate agencies at each location.

I. Meteorology and Other Atmospheric Measurements

There are 5 meteorological (met) towers located throughout the Los Alamos, DOE complex. The closest station to TA-33 Point is located at TA-54, approximately 6 km to the NNE. The second closest is located at TA-49. approximately 7 km, NW of the Point. As described in detail elsewhere, the Portable Plume Generator (PPG) contains its own portable met station. A second portable met station, similar to the one being used in the PPG, is being purchased for inclusion into the CACDI field platform for local atmospheric measurements. All of these stations log basic weather data, including: temperature, relative humidity, barometric temperature, wind speed and direction. Data from the two portable met stations will be logged directly by the CACDI system DAC (for ground-based experiments). Data from the PPG is transmitted via spread-spectrum radio technology to the base station located aboard the CACDI field platform.

The RSTR has several permanent met station installations, at various heights, near the chemical release apparatus on the lake bed. Data from the station closest to the wind tunnel is transmitted to the lidar test pads via local area network. This Met data will be archived by the LANL Tan Trailer, Generation II DAC

during ground-support of airborne missions. A radiosonde program can be implemented to support atmospheric turbulence measurements. However, the need for such a system and implementation has yet to be investigated. Scintillometers will be employed at both NTS and Los Alamos during AIPs, to assist in quantification of atmospheric conditions during DIAL measurements.

J. Release Apparatus for Airborne AIPs and Ground-based Support Experiments

The NTS Remote Sensor Test Range has wind tunnel and a stack that will be used for CACDI airborne chemical release experiments. The wind tunnel has been used in three previous lidar missions. It develops a horizontal plume approximately 2 meters in diameter which remains fairly homogenous, collimated and well characterized for approximately 20 feet. The wind tunnel provides release concentration data based on mass flow meters, gas analyzers and FTIR measurements. This data is provided digitally, on the local area network, for archiving by the Tan Trailer, Generation II DAC. The wind tunnel can only release chemicals that are easily evaporated and do not condense on the side walls. Figure 31 shows the RSTR wind tunnel.

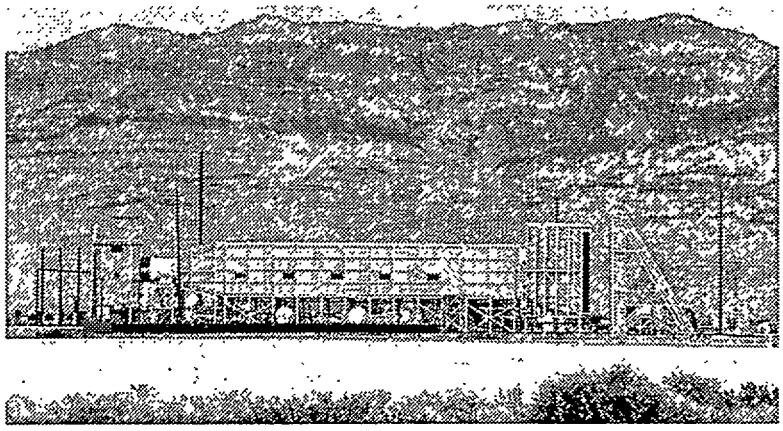

Figure 31. Remote Sensor Test Range Wind Tunnel

There are actually two stacks available for CACDI use; the old, "ETE" stack and a newly engineered stack, currently under construction. The new stack is approximately eighteen inches diameter and 50 feet tall. It was designed and is being installed by the Lawrence Livermore National Laboratory, Resource Team. Actual specifications are forthcoming. The new stack will allow for the release of a greater variety of chemicals relevant to the CALIOPE program. It is engineered to release nearly all of the chemicals desired for CACDI experiments, at rates comparable to those produced by the wind tunnel in the past.

The Portable Plume Generator (PPG) (Figure 32) will be used, when chemical plumes are required, for Los Alamos area AIPs and during routine ground-based experiments. The PPG is a self contained mobile

apparatus capable of generating a small chemical plume, eight (8) inches in diameter, approximately 30 feet above the ground. The PPG utilizes a fume hood to mix the test chemical with air and force it up a stack to be expelled. The fume hood has a volumetric throughput of 420 cubic feet per minute. Flow controllers regulate the flow of gaseous chemicals injected into the fume hood. A variable temperature hot plate is used inside the fume hood to assist in liquid chemical evaporation and expulsion. Electrical components of the fume hood and hot plate are "explosion-proof" in that they either prevent the generation of, or isolate, sparks. The PPG is capable of being remotely controlled via a two-way spread-spectrum radio system. The unit can be remotely operated from distances up to 20 km. The PPG contains an on-board, meteorological tower that measures and reports temperature, relative humidity, barometric pressure, wind speed and direction. The data is displayed both locally and at the base unit, via the spread-spectrum radio. A battery powered data logger is used at the PPG to record and store met data as a backup to the base archive (CACDI or Tan Trailer, Generation II DAC). A 4 kW, on-board, gasoline powered, electrical generator provides power to the PPG. It has fuel capacity for 10 to 12 hours of operation under maximum load.

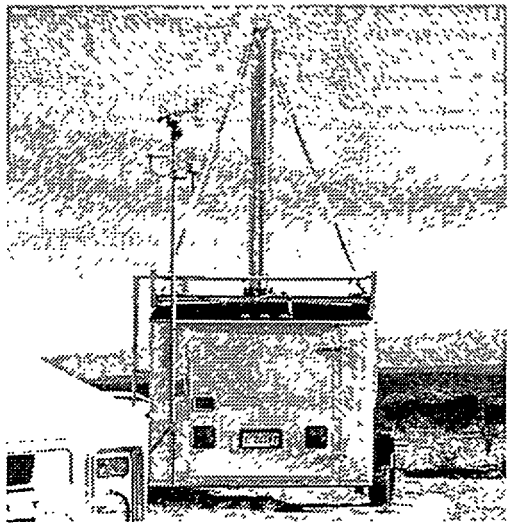

Figure 32. Portable plume generator (PPG)

K. Environment, Safety and Health (ES&H) Issues related to AIPs and Ground-based CACDI

The Department of Energy requires a National Environmental Protection Act (NEPA) review for all experiment activity conducted by LANL. In accordance with policy, this has been done for the CALIOPE Project and approval to proceed has been granted by DOE. Document "DOE IDENTIFICATION NUMBER LAN-94-042," dated 17 January, 1995, concerns chemical releases at Los Alamos. Document "DOE IDENTIFICATION NUMBER LAN-93-0048," dated 1 November, 1993, concerns general laser operation.

Los Alamos National Laboratory requires that a Standard Operating Procedure (SOP) be generated prior to performing potentially hazardous activities. The SOP describes potential hazardous activities and prescribes control measures for mitigation of the hazards. It also prescribes appropriate training for personnel, based on the hazards encountered. The USAF requires Operation Instructions that serve a similar function. CALIOPE personnel will generate appropriate CACDI SOP's for approval by LANL ES&H officials. For airborne operations, the SOP will be submitted to Phillips Laboratory for their approval and inclusion into the Argus Operating Instruction.

Additional training and periodic update briefings are required for personnel involved with airborne missions. They include:

- Annual medical physicals performed by USAF medical staff at Kirtland AFB.
- Land and water survival training, performed by USAF staff at Kirtland AFB.
- Altitude certification performed regionally at Peterson AFB, Colorado Springs, Colorado

For those working on the Argus aircraft, whether they fly or not, these individuals must take the following training:

- Egress training specific to Argus.
- Hazards training specific to the experiment.
- Laser training from the Argus Laser Safety Officer.
- If handling cryogenic fluids, you must have training from the Argus Cryogenics Safety Officer.
- Argus walk around.

A six flight waiver is available for those who are not required to fly on all CACDI missions and will not be working on the aircraft while on the ground.

X. Experimental Plan

A. Introduction

The principal objective of LANL CACDI tests (FY97 and FY98) are to demonstrate the range, sensitivity, and selectivity required for proliferation detection with second generation airborne DIAL systems. These second generation systems include CO_2 lasers operating at pulse repetition frequencies and line-to-line tuning rates up to 10 kilohertz (kHz), background limited receivers, and real-time data analysis (to include chemometric analysis).

Tan Trailer, Generation II will be used at the Los Alamos lidar range to investigate and resolve technical issues which became apparent during its initial fielding at NTS in May 1996 and during the 1996 N-ABLE field campaigns. Tasks include field testing of hardware and software modifications, and testing of improved DIAL and chemometric data analysis algorithms. In support of CACDI airborne tests in 1997 and 1998, Tan Trailer, Generation II will be utilized both as a DIAL platform to provide ground truth information and as a test bed to address technical issues that will be encountered during future field tests

The CACDI airborne lidar will be thoroughly ground tested from a transportable trailer at the Los Alamos lidar range during the summer of 1997. A series of initial flight experiments will be carried out during November at local field test ranges (Albuquerque and Los Alamos) to insure proper operation aboard the aircraft. During the period of January to May of 1998, the CACDI system will be modified and improved based on lessons learned from the initial airborne experiments. This phase of CACDI system development will be implemented in conjunction with a series of local ground tests at Los Alamos, TA-33. A second set of airborne tests will follow at NTS, RSTR in May and June of 1998 to demonstrate chemical plume detection from an airborne platform. Upon the completion of the NTS airborne experimental campaign, a period of approximately two months will be devoted to upgrading the system to optimize DIAL system performance. These modifications may include the addition of advanced chemical plume detection and location methods, such as the use of optimized chemical analysis algorithms and the addition of an IR camera or a receiver based on a multi-element detector. A third series of flight tests will follow in September 1998 to demonstrate airborne DIAL chemical detection capability at a more realistic site (location to be determined), mainly to simulate more humid conditions, and to assess background interference caused industrial or chemical processing plants.

The objectives and schedules for these activities are listed below.

B. Test Objectives and Activities

1. Ground Tests

Tan Trailer, Generation II Test Objectives:

- Improve the capabilities of current 2nd generation CO_2 DIAL systems and mitigate issues associated with "lessons learned" from 1996 and future field campaigns.
- Support the development of more advanced DIAL platforms, including subsequent generations of the CACDI system and advanced imaging CO_2 DIAL systems.

Tan Trailer, Generation II Experiments:

- Determine optimum performance of the existing 2nd generation CO_2 DIAL system.
- Verify current model predictions of system performance and identify limiting noise sources.
- Evaluate proposed subsystem modifications and advanced data analysis techniques such as cooled reference detectors, and chemometric and statistical analysis algorithms.
- Investigate airborne-relevant phenomena and mitigation techniques including background subtraction techniques, and atmospheric/albedo/speckle noise mitigation.
- Demonstrate improved long-range performance with natural and artificial targets.
- Investigate spatially resolved DIAL using focal plane array detectors.

Tan Trailer, Generation II Test Locations:

Los Alamos test range at TA-33 throughout 1997 and 1998 (except the months required to support CACDI flight tests).

CACDI Ground Test Objectives:

- Evaluate basic system performance characteristics, such as laser energy and divergence, wavelength calibration, laser and receiver alignment and stability, and receiver field of view (FOV).
- Assess lidar system control hardware and software upgrades as well as optimize data acquisition and retrieval procedures.
- Evaluate recently developed data processing and analysis algorithms that will allow near real-time visualization of DIAL detection performance aboard Argus.
- Conduct integrated DIAL measurements to determine CACDI system performance using test chemicals.

CACDI Ground Test Experiments:

- Lidar system integration and checkout.
    - Transmitter/receiver subsystems function checkout.
    - Data acquisition, control, storage, and retrieval subsystem function checkout.
    - Development procedures for aligning the laser to the receiver and the visible acquisition cameras.
- System Characterization and Optimization
    - Lidar system alignment checkout and optimization - alignment adjustment and refinement.

- Transmitter and receiver characterization including automatic range gate operation.
- Data acquisition and control electronics characterization with real signals.
- Signal strength and SNR measurements at several ranges.
- Multiple laser wavelength SNR measurements.
- Characterize thermal and vibrational stability of the CACDI system.
- Compare experimental and model results.
- Optimize data acquisition and processing procedures.

- DIAL Tests with Chemical Absorption
  - DIAL measurements with a calibrated chemical medium.
  - Chemical plume detection demonstration.
  - Compare experimental and model results.
  - Optimal chemical detection strategy development

- System Modification and Improvement Implementation and Evaluation.
  - Modifications and improvements implementation.
  - Evaluation and documentation of improvements.

CACDI Ground Test Locations:

Los Alamos test range at TA-33 using a transportable trailer to begin in July 1997, and Kirtland AFB aboard ARGUS prior to each airborne test campaign.

2. Airborne Tests

CACDI Airborne Test Objectives:

- Demonstrate predicted single-shot system performance from an airborne platform using high repetition rate, low pulse energy lasers and an improved sensitivity receiver (1997).
- Demonstrate sensitivity enhancement through shot averaging in the presence of albedo, atmospheric and geometric variations using fast-tuning lasers (1997 - 1998).
- Demonstrate chemical identification for pulsed and continuous plume observations (1998).

CACDI Airborne Test Experiments:

The CACDI flights are primarily to accomplish the following test measurements:

- Flight operations checkout and assessment including pointing, tracking, and ranging issues.
- Benchmark single-shot and shot-averaged system performance at various ranges between 7.5 and 20 km.
- Measure spectral characteristics of albedo/atmospheric variations observed while orbiting a target.
- Conduct on/off plume measurements to evaluate chemical detection limits using real-time averaging, background reduction, and chemometric algorithms.
- Collect data while scanning the lidar beam across the plume to evaluate plume location and background subtraction methods.

CACDI Flight Test Locations:

There are three segments to CACDI airborne field experiments:

- Local airborne exercises and experiments conducted around Los Alamos at TA-33 test range, and Kirtland AFB (near Pad 4, the exact location is not yet determined) with possibly one exploratory flight at Nevada Test Site (NTS) Remote Sensor Test Range (RSTR).
- Nevada Test Site, 1998 RSTR campaign during the months of May and June
- Airborne DIAL chemical detection capability and operational scenario demonstration at a more realistic site (location yet to be determined, possible sites: CART, Allied Signal Kansas City Plant, and Savannah River Site.).

C. Top Level CACDI Field Experiment Test Schedule

A general test schedule is outlined below. A more detailed schedule is provided in the CACDI Experimental Plan.

	FY97												FY98											
General Tasks	O	N	D	J	F	M	A	M	J	J	A	S	O	N	D	J	F	M	A	M	J	J	A	S
Tan Trailer, Generation II DIAL Tests																								
CACDI Ground Tests																								
CACDI Airborne Tests																								

Figure 33. Top Level CACDI Field Experiment Test Schedule